Petroleum Science 19 (2022) 929–948

Contents lists available at ScienceDirect

Petroleum Science

journal homepage: www.keaipublishing.com/en/journals/petroleum-science

Original Paper

Sedimentary characteristics and implications for hydrocarbon exploration in a retrograding shallow-water delta: An example from the fourth member of the Cretaceous Quantou Formation in the Sanzhao depression, Songliao Basin, NE China

Quan-Sheng Cai [a, b], Ming-Yi Hu [a, b], Yi-Ni Liu [a, *], Oumar-Ibrahima Kane [a], Qing-Jie Deng [a], Zhong-Gui Hu [a], Hua Li [a], Ngong-Roger Ngia [a, c]

[a] School of Geosciences, Yangtze University, Wuhan, Hubei 430100, China
[b] Key Laboratory of Exploration Technologies for Oil and Gas Resources, Ministry of Education, Yangtze University, Wuhan, Hubei 430100, China
[c] Department of Geology, University of Buea, P. O. Box. 63, Buea, Cameroon

ARTICLE INFO

Article history:
Received 19 August 2020
Accepted 15 November 2021
Available online 27 January 2022

Edited by Jie Hao and Teng Zhu

Keywords:
Depositional environment
Retrograding shallow-water delta
Lake level fluctuation
Channel sandstone
Hydrocarbon exploration
K_2q^4
Songliao Basin

ABSTRACT

Based on the analysis of core, logging, and testing data, the fourth member of the Cretaceous Quantou Formation (K_2q^4) in the Sanzhao depression, Songliao Basin, is investigated in order to understand the sedimentary characteristics and hydrocarbon exploration significance of a retrograding shallow-water delta. The results show that during the sedimentary period of K_2q^4, the Sanzhao depression with a gentle basement experienced stable tectonic subsidence and suffered a long-term lake level rise caused by paleoclimate changes (from semiarid to semihumid), the K_2q^4 in the study area were dominated by a fining-upward deltaic succession and had relatively stable thickness. From the bottom to the top, the color of mudstone gradually changes from purplish-red to gray and grayish-green, the contents of caliche nodules decrease gradually, while the presence of pyrite in sediments becomes frequent. Channel sandstones mainly composed of siltstone and fine sandstone with developed high-energy sedimentary structures constitute the main sand bodies of deltaic deposits, but the scale of channel sandstones decrease upward. Despite the long-term lake level rise and fining-upward sedimentary succession, purplish-red mudstone, caliche nodules and thin channel sandstones are still broadly distributed in the study area, and thin channel sandstones can be found at the top of K_2q^4 covered by the black oil shale of Qingshankou Formation. These assertations suggest that the study area was dominated by retrograding shallow-water delta deposits during the sedimentary period of K_2q^4. In comparison with modern Poyang Lake, we infer that during the sedimentary period of K_2q^4, the study area experienced frequent lake level fluctuations triggered by paleoclimate changes despite the long-term lake level rise, and the lake level fluctuations control the deposition of retrograding shallow-water delta. In addition, most of the thin channel sandstones distributed at the top of K_2q^4 and covered by black oil shale are generally immersed in oil, indicating that the thin channel sandstones formed at the top of a retrograding shallow-water delta sedimentary succession are favorable targets for lithological reservoir exploration.

1. Introduction

Since the concept of “shallow-water delta” was firstly proposed by Fisk et al. (1954), ancient shallow-water deltas without a tripartite structure (Gilbert, 1885) have been found all over the world, such as in the Bohai Bay Basin (Wang et al., 2015; Zeng et al., 2015; Tian et al., 2019; Dou et al., 2020), Junggar Basin (Chen et al., 2015; Liu et al., 2015; Zhao et al., 2015; Zhu et al., 2017a), Late Pleistocene Lake Bonneville (Lemons and Chan, 1999), Mesohellenic Basin (Zelilidis et al., 2002), and Alberta Basin (Reading, 1996; Leckie et al., 2004). As a river-dominated delta with widely distributed sandstones, the shallow-water delta has become an important object for oil and gas exploration and a hotspot for sedimentary research in recent years (Overeem et al., 2003;

* Corresponding author.
E-mail address: lyn953403954@163.com (Y.-N. Liu).

https://doi.org/10.1016/j.petsci.2022.01.018

Fielding et al., 2006; Olariu and Bhattacharya, 2006; Zou et al., 2006; Lee et al., 2007; Zhu et al. 2008, 2012, 2013a, 2013b, 2017a, 2017b; Cai and Zhu, 2011; Wang et al., 2012; Rahman et al., 2014; Deng et al., 2019). Several aspects of the sedimentology of shallow-water deltas have been examined preliminarily: (i) types of depositional basins and tectonic conditions for the development of shallow-water deltas (Donaldson, 1974; Horne et al., 1976; Zhao et al., 2011a; Zhu et al., 2013b, 2017b; Dou et al., 2020; Wang et al., 2020); (ii) source supply systems and formation mechanisms of shallow-water deltas (Hoy and Ridgway, 2003; Cornel and Janok, 2006; Zhu et al. 2012, 2013b, 2017a; Liu et al., 2015; Xin et al., 2019; Tian et al., 2019; Feng et al., 2019); (iii) sedimentary architecture and characteristics of sedimentary facies (Postma, 1990; Lemons and Chan, 1999; Olariu and Bhattacharya, 2006; Zhu et al. 2013a, 2017b; Li et al., 2014; Chen et al., 2015; Zhang et al. 2016, 2018); (iv) types and distribution of sandstone in shallow-water deltas (Lou et al., 1999, 2004; Zou et al., 2008; Cao et al., 2010; Cai and Zhu, 2011; Wang et al., 2012; Rahman et al., 2014; Zhang et al., 2017; Deng et al., 2019). Despite these studies listed above, detailed research on sedimentary characteristics and development models of a retrograding shallow-water delta formed during a long-term lake level rise is lacking, especially the effect of lake level fluctuations on thin channel sandstone distribution near lake center, which is important for lithological reservoir exploration.

The Songliao Basin, with abundant oil and gas resources, is a large-scale Meso-Cenozoic basin in China. Previous researches indicate that the Songliao Basin was mainly dominated by fluvial shallow-water deltaic, and lacustrine environments during the sedimentary period of the Upper Cretaceous Quantou Formation (K_2q), and the basin experienced a noticeable lake level rise since the deposition of the 4th member of the Quantou Formation (K_2q^4) (Cai and Zhu, 2011; Pan et al., 2012; Zhu et al., 2012; Meng et al., 2016; Deng et al., 2019). Despite the long-term lake level rise and the gradual retrogradation of shallow-water delta, thin sandstone of K_2q^4 is still widespread in the basin and plenty of shallow-water deltaic sandstone develops even in the Sanzhao depression located in the central part of the Songliao Basin (Liu et al., 2009; Zhu et al., 2012; Lin and Hou, 2014; Cai et al., 2016; Deng et al., 2019). Moreover, in recent years, many drilled wells from the Sanzhao depression revealed that the thin sandstone that occurred at the top of K_2q^4 usually has good hydrocarbon indication (Liu et al., 2009; Li et al., 2013; Xi et al., 2015; Zhang et al., 2017, 2018; Zhu et al., 2017b; Deng et al., 2019). However, little attention has been paid to the formation mechanism of these widely distributed thin deltaic sandstone formed during a long-term lake level rise period, as well as its petroleum exploration potential.

Therefore, the K_2q^4 in the Sanzhao depression was taken as a research object, and this paper aims to document the sedimentary characteristics of K_2q^4 and gain insights into the depositional processes of a retrograding shallow-water deltaic system and discuss its exploration potential. The specific objectives are as follows: (i) document lithofacies types and facies assemblages presented in K_2q^4; (ii) present the characteristics of sedimentary environment evolution of K_2q^4; (iii) analyze the lake level changes and develop a depositional model for a retrograding shallow-water; (iv) discuss the formation mechanism of the widely developed thin sandstone in a retrograding shallow-water delta, as well as its significance for oil and gas exploration.

2. Geological backgrounds

Located in the northeastern part of China, the Songliao Basin is a Meso-Cenozoic petroliferous basin with an area of 26×10^4 km^2 (Fig. 1a). According to the basin's internal structures, it can be divided into six first-order tectonic units, namely the West Slope, North Slope, Northeast Uplift, Central Depression, Southeast Uplift, and Southwest Uplift (Feng et al., 2010; Meng et al., 2016). The study area, as one of the most oil-rich areas, is present in the central part of the Central Depression, namely the Sanzhao depression (Fig. 1).

Previous studies indicate that the Songliao Basin experiences three distinct stages of basin evolution: (i) a rifting stage (J_3-K_1), (ii) a subsidence stage (K_1−K_2), and (iii) a tectonic reverse stage (K_2-Q) (Feng et al., 2010; Wei et al., 2010; Sorokin et al., 2013; Cai et al., 2017) (Fig. 2). Sediments within the basin can be divided into three tectonostratigraphic units corresponding to the three tectonic stages: lower rifting strata, middle subsidence strata, and upper inversion strata (Wei et al., 2010; Li et al., 2012; Meng et al., 2016; Cai et al., 2017; Deng et al., 2019). The total thickness of these strata in the study area commonly exceeds 5000 m (Feng et al., 2010) (Fig. 1c).

The Upper Cretaceous Quantou Formation (K_2q) in the Sanzhao depression was formed during the stable subsidence stage, and it can be further divided into four members: K_2q^1, K_2q^2, K_2q^3, and K_2q^4 (Fig. 2). During the sedimentary stage of K_2q^4, the study area had a gentle slope on paleogeomorphology which was less than 1° (Zhu et al., 2012), and there were two provenance supply systems according to different compositions of heavy minerals in the northern and southern parts (Li et al., 2012) (Fig. 1b). Meanwhile, the sedimentary stage of K_2q^4 was a period of extreme greenhouse warmth with a slight decrease in temperature, the paleoclimate of the Songliao Basin at that time was changed gradually from semiarid to semihumid leading to long-term lake level rise (Wu et al., 2009; Zhu et al. 2012, 2017b; Wang et al., 2013; Zhao et al., 2014; Jones et al., 2018; Yang, 2018). Therefore, the K_2q^4 in the study area is mainly dominated by deltaic and lacustrine sediments with an approximate thickness of 90 m (Cai et al., 2016; Deng et al., 2019), and it shows a fining-upward succession which is covered by the black oil shale of K_2qn^1 (Figs. 1c and 2).

Based on the analysis of lithological succession, paleoclimate, and lake-level changes, the K_2q^4 was divided into a lacustrine transgressive systems tract (LTST) of a 3rd order sequence by previous researchers (Li et al., 2007; Wu et al., 2009; Feng et al., 2010; Hu et al., 2015; Meng et al., 2016; Cai et al., 2016; Sun et al., 2017; ; Lai et al., 2017; Deng et al., 2018, 2019) (Fig. 2a). The bottom boundary of the LTST is the interface between K_2q^4 and K_2q^3, which is characterized by widely developed publish-red mudstone and channel erosion surface (Zhu et al., 2012; Sun et al., 2017; Deng et al., 2018); the top boundary of the LTST marked by the black oil shale of the K_2qn^1 represents a maximum flooding surface of a third-order sequence (Fig. 2b). Based on sedimentary succession, the K_2q^4 is usually subdivided into three fourth-order sequences (Sq1-Sq3) (Li et al., 2007; Hu et al., 2015; Cai et al., 2016; Sun et al., 2017; Deng et al., 2018, 2019), of which the lower two 4th order sequences are composed of LTST and LRST (lacustrine regressive systems tract), and the upper one consists of LTST (Fig. 2b).

3. Materials and methods

This study focuses on the K_2q^4 in the Sanzhao depression, where established petroleum wells are abundant. Most data presented in this research including well logs, cores, and testing data (granularity, rock composition, and major elements) were provided by the Exploration and Development Research Institute of Daqing Oilfield Co Ltd. Partial data related to Poyang Lake were compiled from previous research results and China's National Satellite Meteorological Centre (Zhang et al., 2012; Deng et al., 2015; Liang et al., 2016). First, the grain-size data from 164 samples within 22 wells and the rock composition data from 234 samples within 28 wells were used for petrologic analysis. Then, well logs and cuttings from 216 wells were also examined for the analysis of the depositional environment, as well as the sedimentological data (lithology,

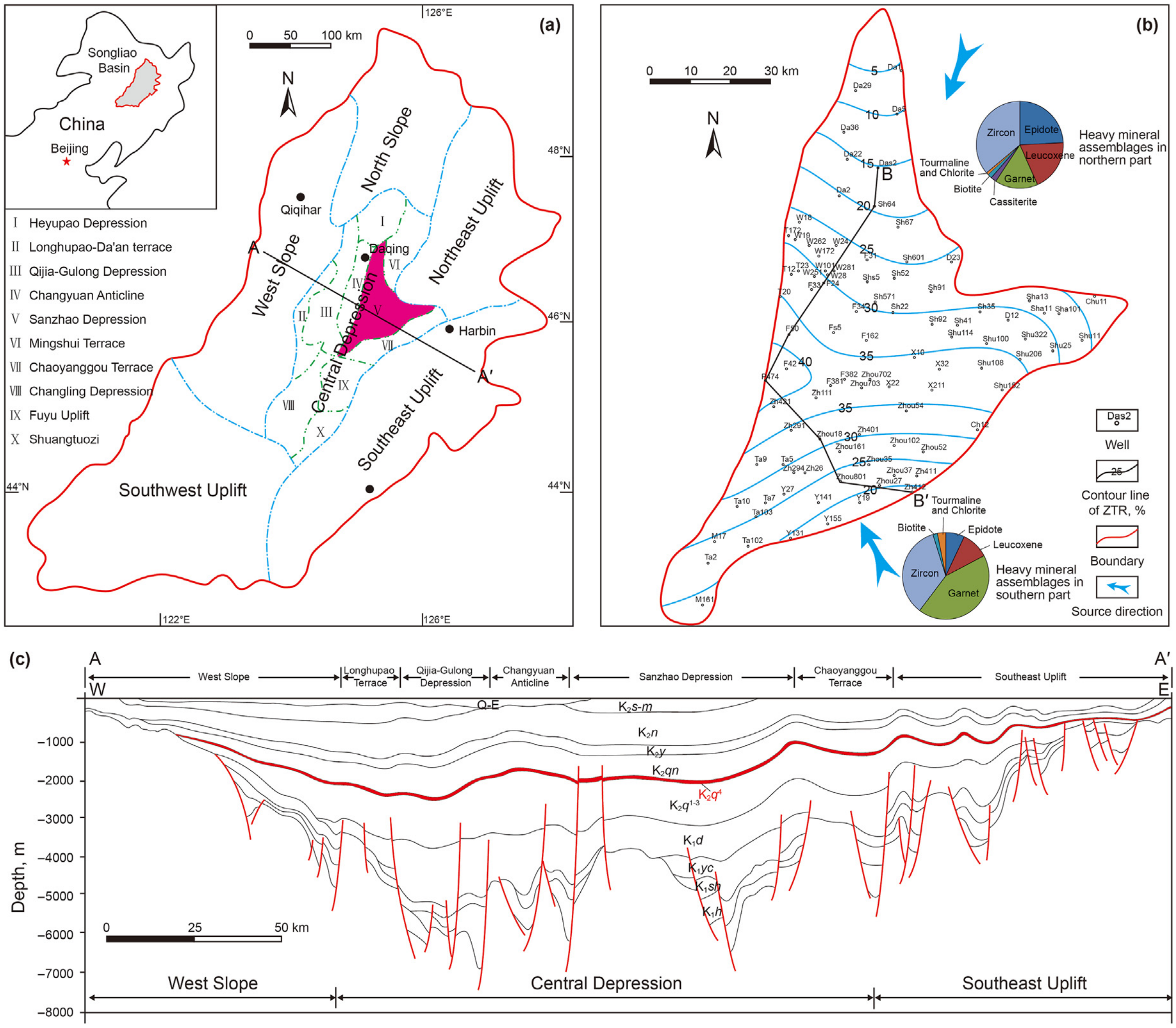

Fig. 1. (**a**) Location map of the Sanzhao depression and tectonic units of the Songliao Basin. The black line (AA′) shows the location of the stratigraphic profile (Fig. 1**c**) of the Songliao Basin. (**b**) Key well locations and characteristics of heavy minerals showing the provenance systems of the Sanzhao depression during the sedimentary stage of K_2q^4 (the contour line of ZTR is modified from Liu et al., 2012). ZTR-The total content of zircon, tourmaline, and rutile within transparent heavy minerals. The solid line (BB′) shows the location of the well-correlation profile (Fig. 9). (**c**) Stratigraphic section across the central part of the Songliao Basin showing the basin structure and distribution of K_2q^4 (modified from Feng et al., 2010).

sedimentary structures, and fossil content) obtained through observation and description of cores from 51 wells. According to the development characteristics of mudstone and antigenic minerals, lake level fluctuations during the sedimentary period of K_2q^4 are discussed along with the major elements analysis and by comparison with water changes in the modern Poyang Lake. Apart from these attempts, based on the analysis of lake level fluctuations and sedimentary characteristics, we develop depositional models for the retrograding shallow-water delta deposition of K_2q^4. Finally, the formation mechanisms of widely distributed thin channel sandstone in a retrograding shallow-water delta are also discussed, as well as the significance for the oil and gas exploration of thin sandstone bodies developed at the top of a retrograding shallow-water deltaic succession.

4. Results

4.1. Petrography and texture

The lithology of K_2q^4 in the study area is broadly characterized by gray to light gray fine sandstone and siltstone, purplish-red and grayish-green mudstone, and the color of mudstone in K_2q^4 is gradually changed from purplish-red to grayish-green from the bottom to the top. Analysis of core samples reveals that there are nine types of sedimentary fabrics: quartz grains, feldspathic grains (both orthoclase and plagioclase), rock fragments, mud, calcite cement, pyrite, kaolinite, anhydrite, and surface porosity. The detrital components, composed of 21–37% quartz (with an average of 29.2%), 27–43% feldspar (averaging 35.1%), and 24–52% rock fragments (with an average of 35.7%), indicates that the sandstone and siltstone are feldspathic litharenite and lithic arkose (Folk, 1974) (Fig. 3a). Lithic fragments are igneous in composition. Moreover, the content of mud matrix in sandstone samples ranges from 2% to 22% (averaging 8.1%). These data show that the sandstone of the K_2q^4 in the study area has low compositional maturity and similar mineral composition (Fig. 3a).

The grain-size of clastic particles in the samples ranges from 0.01 to 0.39 mm, and approximately 86% of coarse deposits have a median grain diameter between 0.01 mm and 0.0625 mm (siltstone); 14% have a median grain diameter between 0.0625 mm and 0.125 mm (fine sandstone) (Fig. 3b). In addition, the C value on the grain-size accumulation probability curve correlates well with M

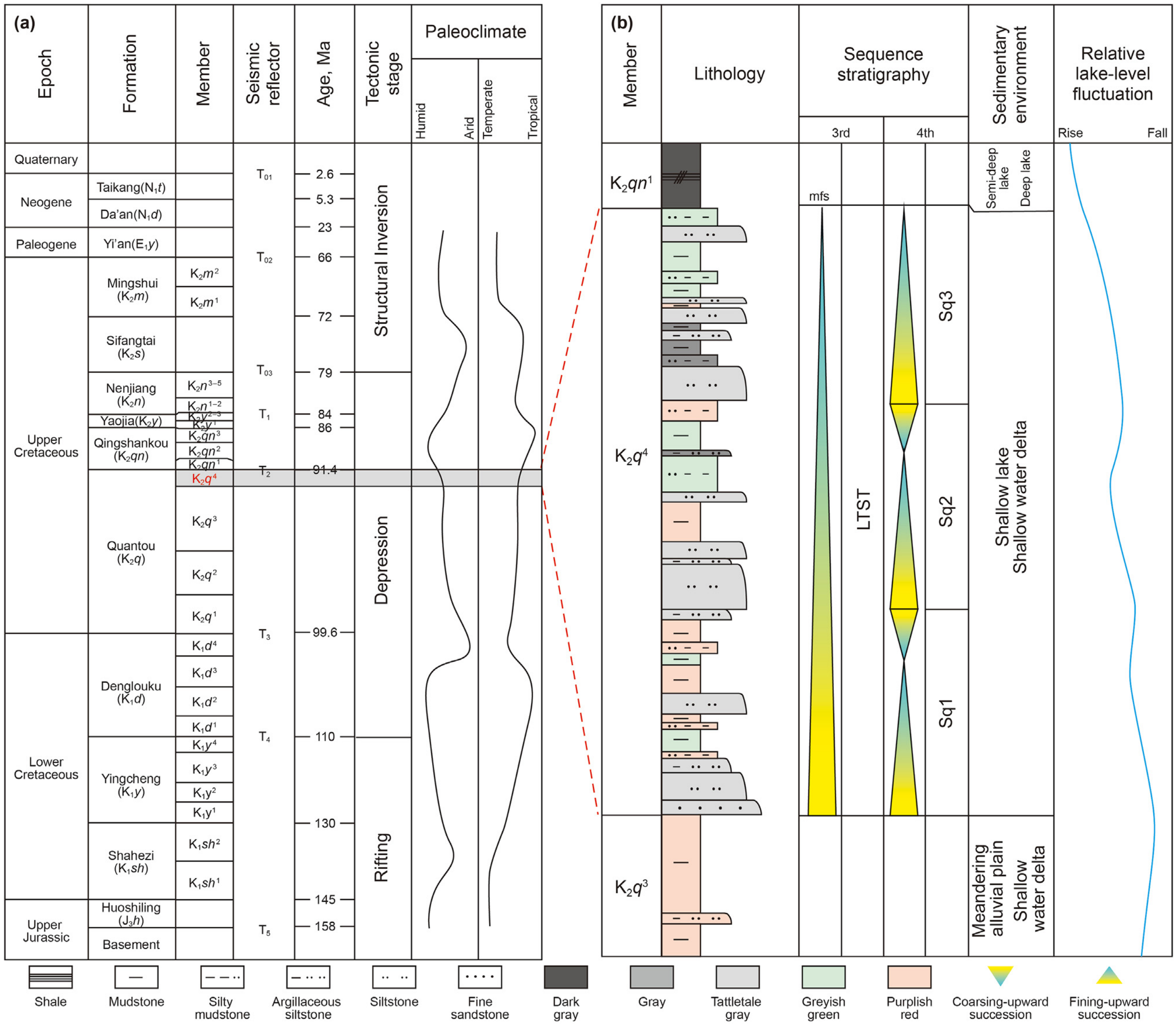

Fig. 2. (**a**) Stratigraphic units and paleoclimate changes of the Songliao Basin (modified from Wu et al., 2009 and Wang et al., 2013). (**b**) Detailed K_2q^4 stratigraphy in the Sanzhao depression showing the lithological succession, sequence stratigraphy, and sedimentary environments. Sq-4th order sequence.

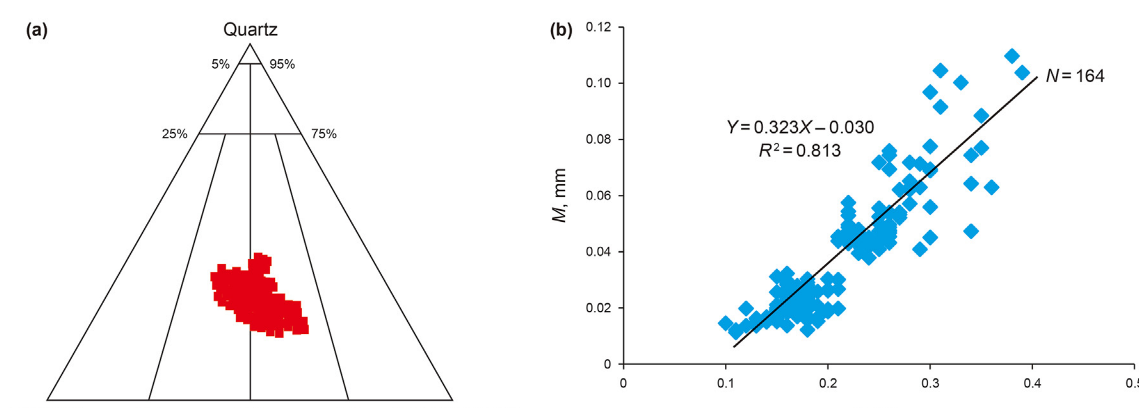

Fig. 3. (**a**) Detrital composition of sandstone samples (including siltstone) from K_2q^4 of the Sanzhao depression, based on the classification of Folk (1974). (**b**) Grain-size features of sandstone samples (including siltstone) from K_2q^4 in the Sanzhao depression. M-Particle diameter corresponding to 50% on grain-size accumulation probability curve. C-Particle diameter corresponding to 1% on grain-size accumulation probability curve.

(Fig. 3b), and thin-section analysis reveals that most clastic particles are sub-rounded. These data indicate that most of the fine sandstone and siltstone in K_2q^4 have moderate textural maturity resulting from a deposition with a relatively long transportation distance.

4.2. Major elements

20 samples mainly collected from the K_2q^4-sq1 mudstone in the Well Sheng 41 were analyzed to determine the composition of major elements (Table 1). The results indicate that SiO_2 and Al_2O_3 are the primary constituents for K_2q^4-sq1 mudstone. Almost all oxidizing material contents show numerical fluctuations (Table 1). The chemical index of alteration (CIA) calculated by Al_2O_3/(Al_2O_3+Na_2O + CaO*+K_2O), is often used as an indirect proxy of climate change (Nesbitt and Young, 1982), and the ratio of Fe/Mn is used to represent water depth of a lake (Tian et al., 2006), which are listed in Table 1. CIA values, ranging from 71.67 to 77.49, slightly increase upward and show obvious fluctuations. The ratio of Fe/Mn ranges from 249.87 to 11.47, with an average of 89.91, and shows frequent fluctuations (Table 1, Fig. 11).

4.3. Facies analysis and environment interpretation

By the observation and description of cores in the study area and its periphery, nineteen lithologic facies are classified based on lithology, sedimentary structure, grain size, fossil content, and some authigenic minerals (Table 2). According to sedimentary characteristics of different environments and the combination of the above lithologic facies, four facies assemblages have been grouped (FA1-FA4) and they represent shallow lacustrine environment, shallow-water delta front, shallow-water delta plain, and meandering river, respectively.

4.3.1. Facies assemblage 1 (FA1)

4.3.1.1. Description. FA1 is generally dominated by gray and grayish-green mudstone (Fig. 4a), including Mm, Mp, Mf, MSbp, Msw, and some SAd. Caliche-nodule bearing mudstone is comparatively uncommon (Fig. 4a). Siltstone layers are commonly less than 0.2 m in thickness and are interlaced with gray or grayish-green mudstone layers. Pyrite in the mudstone is dispersed distributed and has a diameter less than 1 cm (Fig. 5c). Fossils in FA1 are mainly comprised of small shells and their molds with a diameter less than 1 cm (Fig. 5d), as well as phytoclasts (Fig. 5e). As the log response to FA1, the GR valve of mudstone is usually high, while that of thin siltstone is relatively low and appears finger-like (Fig. 4a). Moreover, numerous inversed sedimentary cycles can be recognized based on GR variation trends and sedimentary succession (Fig. 4a). According to the logging data and core observation, FA1 is locally distributed at the upper part of the K_2q^4 (Sq3) in the western study area and is generally covered by the black oil shale of K_2qn^1 (Fig. 2b).

4.3.1.2. Interpretation. FA1 dominated by reverse cycle sequence and fine deposits is indicative of a shallow lacustrine depositional system. Thick (1–3 m) gray and grayish-green mudstone is formed under subaqueous reducing conditions with low energy, which is illustrated by the widely developed pyrite within mudstone. The abundant fossils including shells and phytoclasts are indicative of normal-salinity lake conditions (Heckel, 1972). The thin-bedded argillaceous siltstone, representing a relatively high-energy condition, is migrated from the delta front or shallow-water sand bodies near shore due to wave action (Lemons and Chan, 1999; Reading, 1996; Zhu et al., 2012, 2017b; Zhang et al., 2018; Deng et al., 2019). Occasionally caliche-nodule bearing mudstone is usually formed in restricted shallow-water areas, indicating that the lake water in the study area is shallow and experiences lake-level fluctuations (Zhu et al., 2012).

4.3.2. Facies assemblage 2 (FA2)

4.3.2.1. Description. FA2 is dominated by gray to grayish-green mudstone, gray siltstone (Fig. 4b). Mudstone in FA2 includes Mm, Mp, MSbp, Mc and Msw (Fig. 5c, h, i). Pyrite particles within the gray argillaceous siltstone are distributed sporadically (Fig. 6a). FA2 also contains thin beds deformed argillaceous siltstone (Fig. 6b). Caliche nodules in grayish-green mudstone are common when compared with FA1. The thickness of coarse deposits mainly composed of Stw, Sp, Sm, Scr and Smc is commonly less than 2.5 m, and generally show a fining-upward succession (Fig. 4b). Erosion surfaces and some small grayish-green mud clasts are locally present at the bottom of siltstone layers (Fig. 6d). Moreover, reverse graded siltstone (usually less than 0.15 m in thickness) can be recognized (Figs. 4b and 6c). According to the logging data and core observation, FA2 is dominated by normal sedimentary cycle and

Table 1
Composition of major elements and geochemical proxies of mudstone from K_2q^4 and K_2qn in the Well Sheng 41 within the Sanzhao depression, Songliao Basin.

Depth, m	Formation	Al_2O_3, %	SiO_2, %	K_2O, %	CaO, %	TiO_2, %	MnO_2, %	Fe_2O_3, %	P_2O_5, %	Na_2O, %	MgO, %	Fe/Mn	CIA
1852	K_2qn	15.78	59.52	2.47	3.25	0.72	0.14	7.71	0.08	1.06	2.04	60.98	77.47
1853	K_2qn	17.08	59.40	3.44	3.06	0.76	0.07	5.43	0.07	1.00	1.89	85.89	75.84
1855	K_2q^4-sq1	16.19	65.84	2.96	1.01	0.75	0.05	4.90	0.04	1.27	1.69	108.51	74.64
1857	K_2q^4-sq1	16.87	64.17	3.40	1.84	0.77	0.06	4.48	0.05	1.15	1.65	82.68	74.75
1859	K_2q^4-sq1	16.44	62.40	3.39	1.77	0.78	0.05	5.90	0.06	0.90	2.12	130.66	76.01
1861.4	K_2q^4-sq1	17.27	61.35	4.27	1.78	0.72	0.04	5.50	0.06	0.79	2.06	152.25	74.70
1863	K_2q^4-sq1	17.20	62.28	4.35	1.52	0.70	0.04	5.20	0.04	0.97	1.79	143.95	73.22
1864	K_2q^4-sq1	17.16	57.63	4.12	4.67	0.69	0.09	4.99	0.10	0.95	2.02	61.39	74.03
1865.5	K_2q^4-sq1	15.53	64.89	2.72	2.64	0.71	0.09	4.64	0.09	1.24	1.98	57.09	74.92
1868.4	K_2q^4-sq1	15.99	61.05	3.26	4.83	0.57	0.19	4.18	0.13	0.79	1.66	24.36	76.76
1869.5	K_2q^4-sq1	16.80	63.32	3.89	2.12	0.68	0.08	4.43	0.08	0.84	1.81	61.32	75.10
1872	K_2q^4-sq1	15.75	57.85	3.18	6.03	0.65	0.16	4.54	0.17	0.78	1.79	31.42	76.87
1874	K_2q^4-sq1	15.34	66.48	2.72	1.73	0.72	0.05	4.74	0.07	1.41	1.93	104.97	73.47
1876.6	K_2q^4-sq1	15.69	56.40	3.60	4.58	0.68	0.14	7.44	0.14	0.73	2.29	58.84	75.61
1879	K_2q^4-sq1	15.53	54.36	3.95	6.30	0.58	0.23	5.64	0.20	0.60	1.55	27.15	75.10
1880.6	K_2q^4-sq1	14.84	53.50	2.89	8.28	0.56	0.39	4.04	0.24	0.71	1.53	11.47	77.49
1882	K_2q^4-sq1	16.14	64.82	3.52	2.09	0.68	0.06	4.30	0.08	1.43	1.79	79.35	71.67
1885.4	K_2q^4-sq1	15.83	58.65	3.96	3.67	0.71	0.06	5.98	0.12	0.79	2.03	110.36	74.08
1886.4	K_2q^4-sq1	16.23	59.17	4.29	2.79	0.72	0.05	7.03	0.13	0.86	2.10	155.68	72.98
1889	K_2q^4-sq1	16.65	61.03	4.52	1.62	0.72	0.03	6.77	0.08	0.82	1.98	249.87	72.99

Table 2
Description and interpretation of sedimentary facies of K_2q^4 in the Sanzhao depression, Songliao Basin.

Lithology	Description	Interpretation
Massive mudstone (Mm)	Purplish-red or gray to grayish-green in color; abrupt contact may present between mudstone of different color; friable cores, appears as a paleosol layer, various thickness ranging from 0.2 to 3 m (Fig. 5a and b)	Low-energy conditions. Purplish-red mudstone formed under oxidizing conditions, mostly like in fluvial plain, commonly subaerially exposed; grayish-green mudstone mostly formed under reducing conditions, like swamp, a shallow delta front and lacustrine environments (Olariu and Bhattacharya, 2006; Edmonds et al., 2011)
Pyrite-bearing mudstone (Mp)	Gray, dark gray, and grayish-green in color; pyrite particles with diameter less than 1 cm are distributed dispersedly (Fig. 5c).	Formed under reducing conditions with low energy, mostly like swamp, delta front and shallow lacustrine environment (Reading, 1996; Lemons and Chan, 1999)
Fossil-bearing mudstone (Mf)	Dark gray and grayish-green in color; biological fossils include phytoclasts and shells, concentrated distribution; thickness is less than 5 cm (Fig. 5d and e)	Formed under reducing environment with low energy and quiet setting, e.g., alluvial lake in the delta plain or shallow lacustrine environment (Reading, 1996; Lemons and Chan, 1999; Meng et al., 2016; Zhu et al., 2017b; Deng et al., 2019)
Caliche-nodule bearing mudstone (Mc)	Purplish-red and grayish-green in color; gradually reduced occurrence upward; most carbonaceous materials appeared as off-white caliche nodules, usually with a diameter less than 1 cm (Fig. 5f and g)	Results from low-energy deposition under hot and evaporitic conditions (Zhu et al., 2012, 2017b; Cai et al., 2016; Deng et al., 2019)
Boring pore-bearing silty mudstone (MSbp)	Purplish-red and grayish-green in color; both horizontal and vertical boring pores present, usually with a length less than 10 cm (Fig. 5h)	Formed under relatively low-energy conditions with normal salinity and shallow water, purplish-red color formed by exposed oxidation (Reading, 1996; Zhu et al., 2012; Meng et al., 2016; Deng et al., 2019)
Wave-bedded silty mudstone (MSw)	Purplish-red, gray, and grayish-green in color; asymmetric wavy bedding with low angle; thickness is less than 5 cm (Fig. 5i)	Formed under weak oscillatory environment with low energy, such as flood plain, delta front and shallow lake (Olariu and Bhattacharya, 2006; Edmonds et al., 2011)
Pyrite-bearing argillaceous siltstone (SAp)	Gray in color, homogeneous argillaceous siltstone with a thickness less than 5 cm, pyrite particles are commonly less than 0.5 cm in diameter (Fig. 6a)	Formed by rapid deposition under reducing conditions, mostly like delta front (Reading, 1996; Edmonds et al., 2011; Deng et al., 2019)
Deformed argillaceous siltstone (SAd)	Gray and grayish-green in color; weakly deformed bedding including flame structures, convolute bedding, slump structures and water-escape structures (Fig. 6b)	Results from gravity flow and rapid deposition, probably formed in delta front (Lemons and Chan, 1999; Zhu et al., 2012, 2017b)
Lenticular bedded siltstone (Slb)	Gray thin sandstone surrounded by gray or grayish-green mudstone, usually with a thickness less than 3 cm (Fig. 5i).	Easily formed in delta front and with lacustrine environment with wave activity or the swamp with flood activity (Lemons and Chan, 1999)
Reverse graded siltstone (Srg)	Gray and grayish-green in color; gradually increased grain size and decreased argillaceous matrix upward; with a thickness less than 10 cm (Fig. 6c)	Formed under shallowing water condition, mostly like the sheet sand or distal bar of delta front (Edmonds et al., 2011; Cai et al., 2016)
Current ripple cross-bedded siltstone (Scr)	Purplish-red, gray, and grayish-green in color; unparallel lamina with a total thickness less than 3 cm (Fig. 6d and e).	Channel or levee deposits, most likely in the flanks of distributary channels (Mail et al., 1996; Sahraeyan et al., 2014)
Trough to wedge cross-bedded siltstone (Stw)	Gray and light gray in color; mainly occurs at the lower part of the sandstone; small cross bedding visible (Fig. 6f)	Formed under relatively high-energy conditions, mostly like channel deposits (Bridge, 1993; Olariu and Bhattacharya, 2006; Sahraeyan et al., 2014; Zhu et al., 2017b)
Parallel-bedded siltstone (Sp)	Gray and off-white in color; with a thickness less than 10 cm; usually developed in the lower part of sandstone deposits (Fig. 6g)	Formed under relatively high-energy conditions, mostly like channel deposits (Bridge, 1993; Ghazi and Mountney, 2009)
Massive siltstone (Sm)	Gray and off-white in color; homogeneous or faint lamination; with a thickness less than 10 cm (Fig. 6h)	Rapid deposition of silt, such as channel deposits under changing hydrodynamic conditions (Sahraeyan et al., 2014)
Mud-clast bearing siltstone (Smc)	Gray and off-white in color; grayish-green or purplish-red mud clast with a diameter usually less than 1 cm; decreasing mud clast upward; accompanied with an erosional surface (Fig. 6i)	Formed under high-energy conditions, mostly like lag deposit of channel (Mail et al., 1996; Olariu and Bhattacharya, 2006; Zhu et al., 2012; Deng et al., 2019)
Trough to wedge cross-bedded fine sandstone (FStw)	Light gray and off-white in color; moderate to small cross beds visible; purplish-red argillaceous deposits can be found among laminas; mainly occurs at the lower part of sandstone deposits (Fig. 7a and b)	Formed under high-energy conditions, mostly like channel deposit of delta plain and meandering river environment (Bridge, 1993; Olariu and Bhattacharya, 2006; Cai et al., 2016; Zhu et al., 2012, 2017b)
Parallel-bedded fine sandstone (FSp)	Light gray and off-white in color; purplish-red argillaceous deposits among laminas; mainly occurs at lower part of sandstone deposits; usually accompanied with cross bedding (Fig. 7c)	Formed under high-energy conditions, mostly like channel deposit of delta plain and meandering river environment (Reading, 1996; Ghazi and Mountney, 2009)
Massive fine sandstone (FSm)	Light gray and off-white in color; homogeneous or faint lamination; with a thickness less than 10 cm (Fig. 7d and e)	Rapid deposition of sand, such as channel deposits under changing hydrodynamic conditions (Bridge, 1993; Ghazi and Mountney, 2009)
Mud-clast bearing fine sandstone (FSmc)	Light gray and off-white in color; grayish-green or purplish-red mud clast with a diameter usually less than 2 cm; occurs at the bottom of sandstone deposits; accompanied with an erosional surface (Fig. 7f)	Formed under high-energy conditions, mostly like lag deposit of meandering river and delta plain (Ghazi and Mountney, 2009; Zhu et al., 2012, 2017b)

sedimentary structures including some erosion surfaces, massive bedding, parallel bedding, and small-scale cross-bedding are associated vertically with thick sand layers (Fig. 4b). FA2 is widely distributed in the central to the west Sanzhao depression and mainly occurred at the middle to the upper part of K_2q^4 (Sq2-Sq3).

4.3.2.2. Interpretation. This facies assemblage (FA2) is interpreted as delta front deposits. Thick gray and grayish-green mudstone intercalated by thin siltstone indicating a relatively low-energy environment in the underwater distributary interchannel, and the thin sandstone is the result of subaqueous overbank deposition commonly caused by seasonal floods and lake waves (Reading, 1996; Lemons and Chan, 1999; Xin et al., 2019). Wave-bedded silty mudstone accompanied with thin sandstone suggests fluctuations of lake wave energy (Edmonds et al., 2011). Weakly deformed bedding within argillaceous siltstone indicates that the topographic slope in the study area is gentle. Caliche nodules within the grayish-green mudstone generally formed under evaporitic conditions indicate shallow and restricted lake water, which are the results of lake level decrease caused by climate change (Zhu et al., 2012, 2017a; Cai et al., 2016; Deng et al., 2019). Locally distributed pyrite within gray argillaceous siltstone covered by grayish-green mudstone is indicative of reducing conditions and increasing water depth (Reading, 1996; Edmonds et al., 2011). Thin reverse graded siltstone in thick mudstone can be interpreted as sheet sand deposits, which is the result of channel sandstone

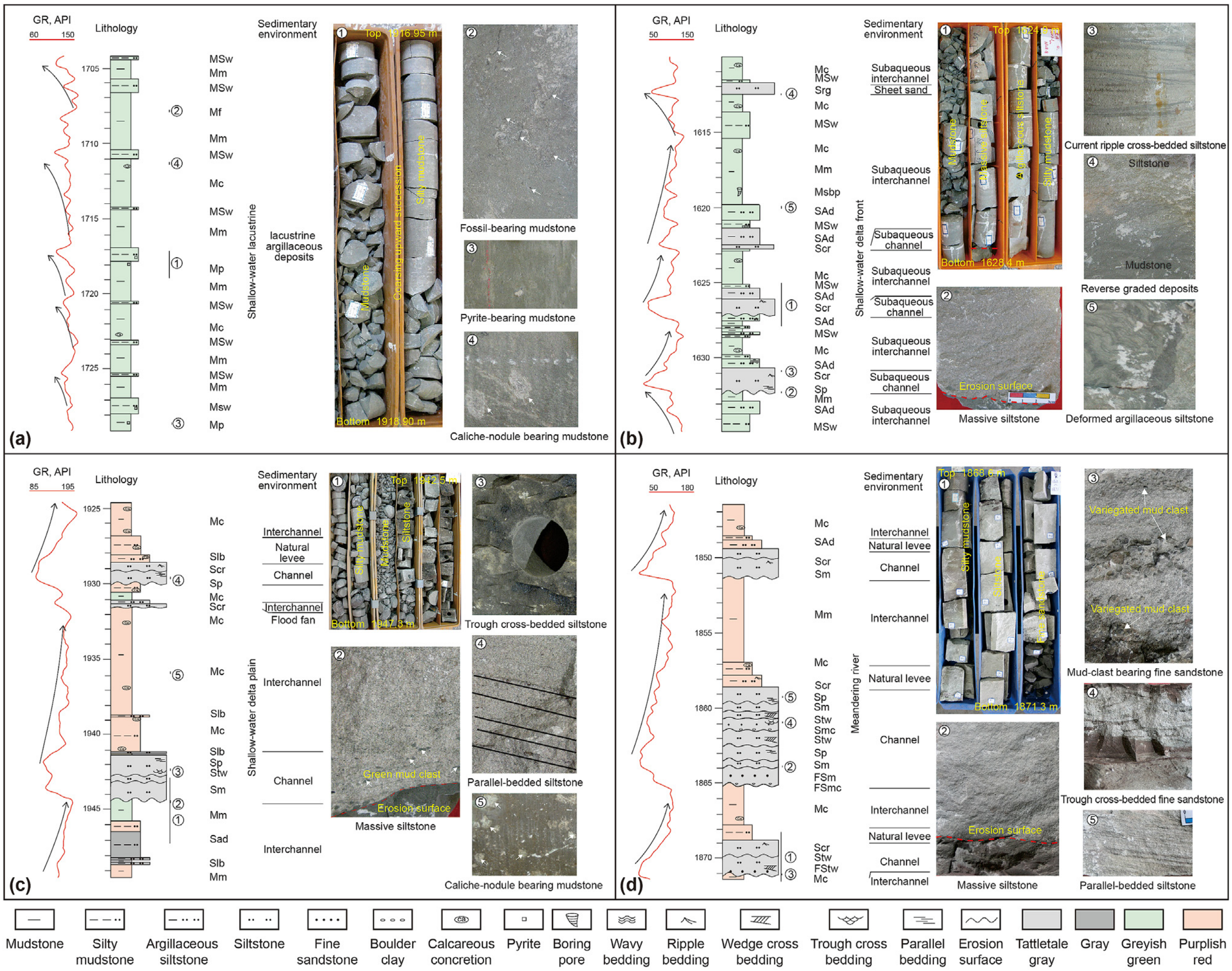

Fig. 4. Four main lithofacies assemblages and their sedimentary interpretations based on core and logging data. (**a**) FA1-Lithofacies assemblages of shallow-water lacustrine deposits from Well P474. (**b**) FA2-Lithofacies assemblages of shallow-water delta front deposits from Well T18. (**c**) FA3-Lithofacies assemblages of shallow-water delta plain deposits from Well Zhou 102. (**d**) FA4-Lithofacies assemblages of meandering river deposits from Well Zh412.

reformation caused by intensifying wave activity (Edmonds et al., 2011). Successive siltstone accompanied with erosion surfaces, massive bedding, parallel bedding, trough to wedge cross-bedding, and some oriented mud clasts suggest the presence of strong directional flow, and these siltstones are the results of subaqueous channel deposition. However, the thickness of successive siltstone is usually less than 2.5 m, and thin channel deposits and grayish-green mudstone are alternated frequently, indicating that underwater distributary channels are not stable in the delta front probably influenced by lake water change.

4.3.3. Facies assemblage 3 (FA3)

4.3.3.1. Description. FA3 consists of purplish-red and gray to grayish-green mudstone including Mm, Mp, Mc, MSbp, and cross-bedded siltstone and fine sandstone including Scr, Stw, Sp, Sm, FStw, FSp, FSm, Smc and FSmc. The FA3 mudstone is characterized by the coexistence of purplish-red mudstone and gray to grayish-green mudstone (Figs. 4c and 5a, and b), which are usually intercalated with thin gray siltstone. Caliche nodules and boring pores are widely distributed in the purplish-red and gray to grayish-green mudstone (Fig. 5f), while pyrite is locally present in the grayish-green mudstone. The thickness of sandstone layers is often more than 3 m, and fine sandstone deposits increase gradually. Sedimentary structures in sandstone layers include cross-bedding (Figs. 6f and 7b), parallel bedding (Fig. 6g), massive bedding (Fig. 6h), and multiple erosion surfaces (Fig. 6h) accompanied by mud clasts (Fig. 6i). Some grayish-green mud clasts (less than 1 cm) are present on parallel beds with a preferred orientation (Fig. 7c). Compared with FA2, erosion surfaces and mud clasts are more common in sandstone layers of the FA3. Successive sandstone including siltstone appear as bell-shaped and small-scale box-shaped curves on gamma logs (Fig. 4c). According to the analysis of logging data and core observation, FA3 is almost distributed in the whole study area and mainly occurred at the middle and lower parts of K_2q^4 (Sq1-Sq2).

4.3.3.2. Interpretation. FA3 represents shallow-water delta plain deposits (Bridge, 1993; Lou et al., 2004; Olariu and Bhattacharya, 2006; Edmonds et al., 2011; Zhu et al., 2012; Cai et al., 2016; Zhang et al., 2018). Gray to grayish-green mudstone and silty mudstone with boring pore and pyrite are indicative of deposition within a low-energy, reducing environment, mostly like swamps, while the purplish-red mudstone formed under oxidizing conditions indicates a dry and hot environment (Lou et al., 2004; Zhu et al., 2012; Wang et al., 2013; Deng et al., 2019), which is consistent with the presence of increased caliche nodules within

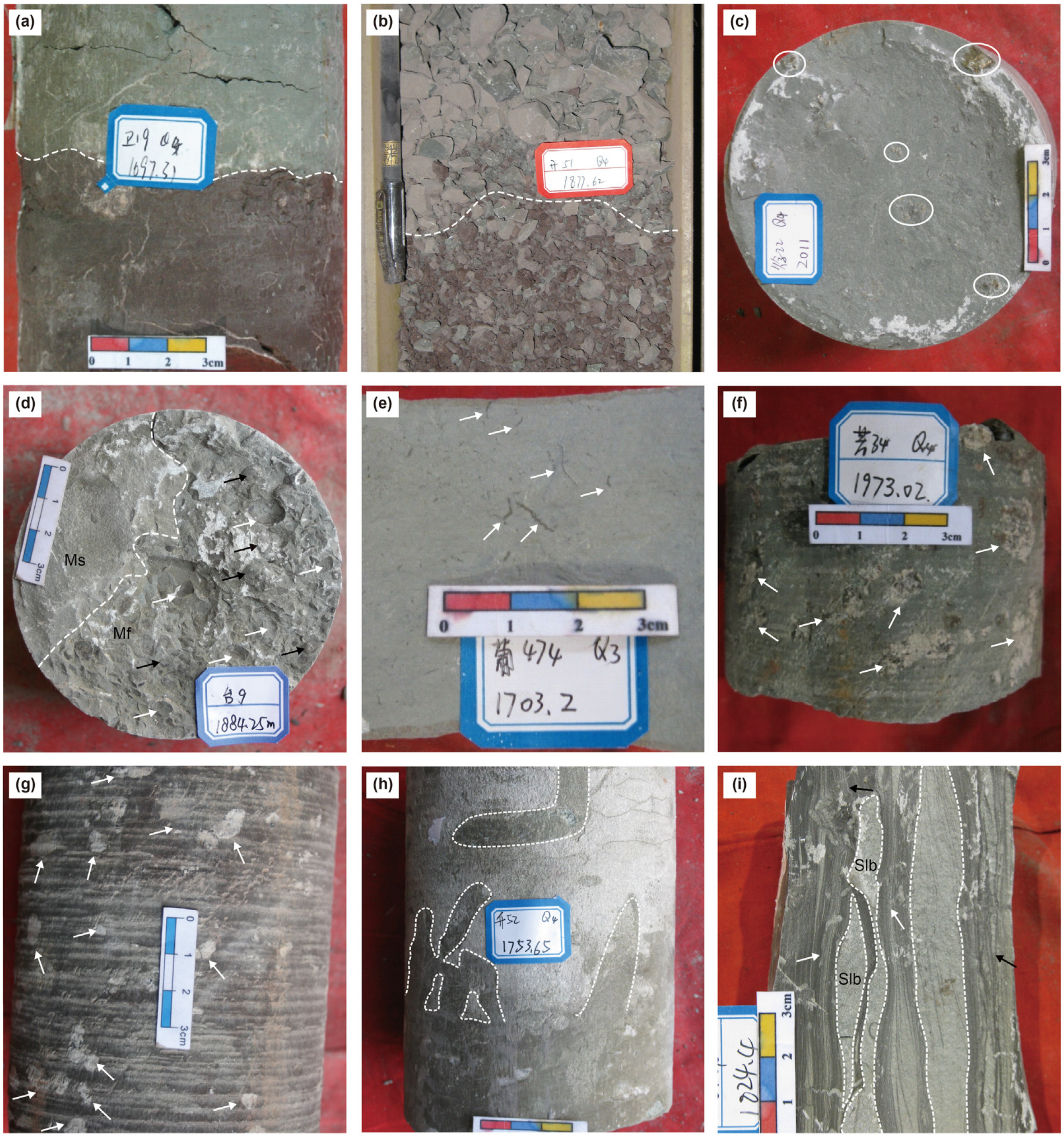

Fig. 5. Core photographs showing the sedimentary characteristics of mudstone in K_2q^4. (**a**) Massive mudstone with different colors; the dotted line indicates their boundary, Well W19 at 1697.31 m. (**b**) Fragmented mudstone with different colors separated by white dotted lines, Well Sh51 at 1877.62 m. (**c**) Pyrite in gray mudstone (white circles), Well X22 at 2011 m. (**d**) Shells fossils (black arrows) and mold fossils (white arrows) in gray mudstone. The white dotted line indicates the boundary between gray massive siltstone and mudstone, Well Ta9 at 1884.25 m. (**e**) Gray mudstone with phytoclasts (white arrows), Well P474 at 1703.2 m. (**f**) Grayish green mudstone with plenty of caliche nodules (white arrows), Well F34 at 1973.02 m. (**g**) Purplish red mudstone with caliche nodules (white arrows), Well Zhou 52 at 1986.02 m. (**h**) Gray silty mudstone with boring pores. The white dotted lines indicate the boundaries of boring pores, Well Sh52 at 1753.65 m. (**i**) Dark gray silty mudstone with gray lenticular siltstone (depicted by white dotted lines). Wave bedding (white arrows) and weakly deformed bedding (black arrows) can be found, Well W281 at 1824.4 m. Slb-lenticular bedded Siltstone. SAd-Deformed argillaceous siltstone. Mf-fossil-bearing mudstone.

purplish-red and grayish-green mudstone. The thick successive sandstone with cross-bedding, parallel bedding, and erosion surfaces are indicative of high-energy distributary channels. The multiple erosion surfaces accompanied by oriented mud clasts are preserved by a mass rapid deposition, showing multiple times of flood activity and channel deposition (Lou et al., 2004; Zhang et al., 2018). Compared with FA2, successive sandstone in FA3 exhibits much more mud clasts and erosion surfaces, and usually has a larger thickness, suggesting that channels in delta plains have better stability. Within FA3, alternations of purplish-red mudstone and grayish-green mudstone demonstrate the fluctuations of paleoclimate and lake level during the sedimentary period of the K_2q^4 (Zhu et al., 2012; Wang et al., 2013; Zhang et al., 2018).

4.3.4. Facies assemblage 4 (FA4)

4.3.4.1. Description. FA4 is characterized by purplish-red dominated mudstone, gray or light gray sandstone including siltstone, and fine sandstone (Fig. 4d). Gray to grayish-green mudstone is less, while purplish-red mudstone is more common and massively bedded (Fig. 4d). Purplish-red caliche-nodule bearing mudstone

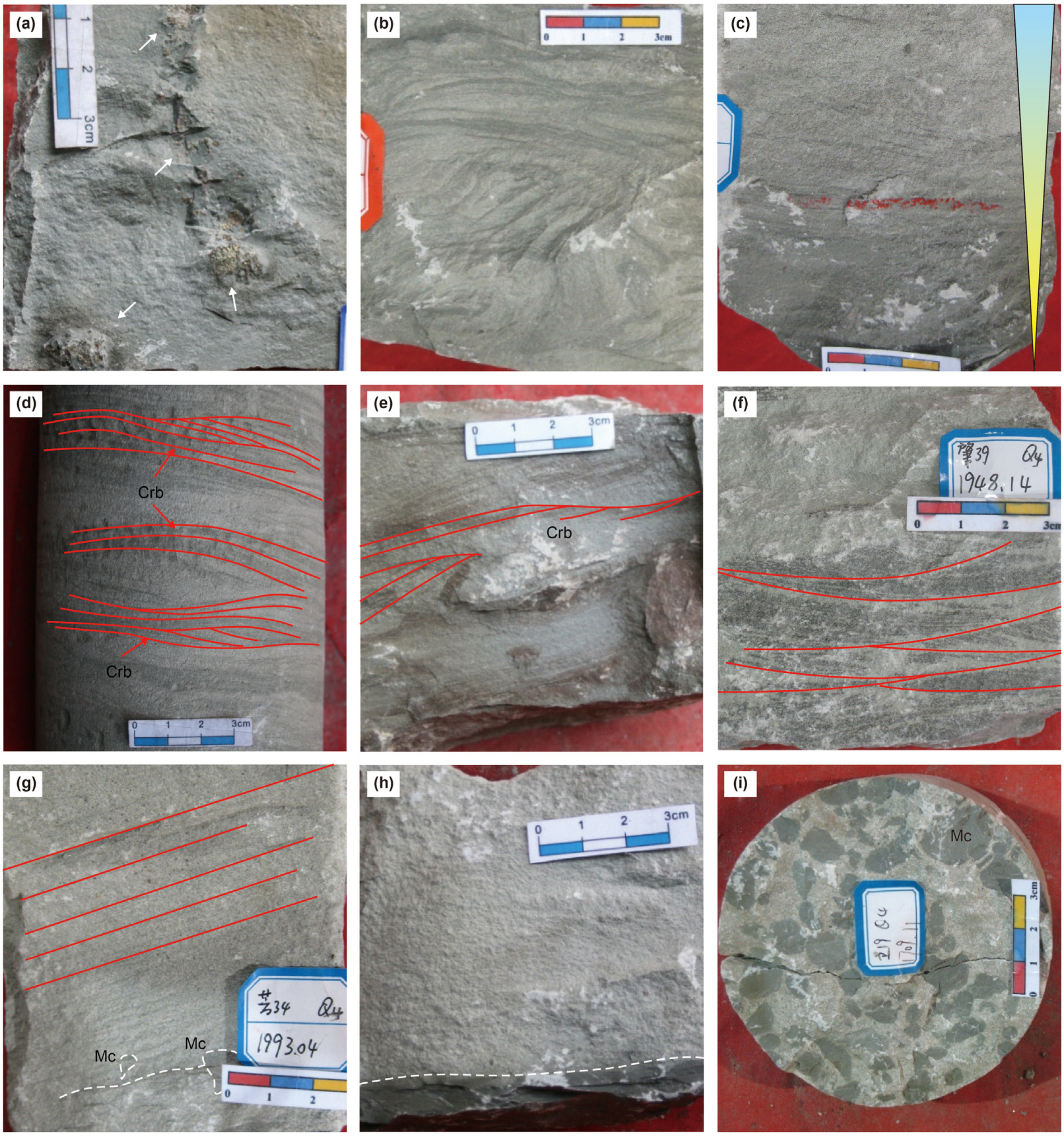

Fig. 6. Core photographs showing sedimentary characteristics of siltstone in K_2q^4. (**a**) Gray argillaceous siltstone with Pyrite (white arrows), Well Y214 at 1639.53 m. (**b**) deformed bedding in grayish-green argillaceous siltstone, Well W19 at 1706.91 m. (**c**) Reverse graded siltstone with gradually changing color from dark gray to gray, Well F33 at 1860.56 m. (**d**) Gray siltstone with climbing ripple bedding, Well Y214 at 1666.19 m. (**e**) Gray siltstone with purplish-red argillaceous deposits. Climbing ripple bedding can be found, Well Zh412 at 1853.03 m. (**f**) The oil-immersed siltstone with trough cross-bedding in the lower part, Well Zh39 at 1948.14 m. (**g**) Light gray parallel-bedded siltstone, scoured surface (white dotted line) with mud clasts (white dotted circles) can be found, Well F34 at 1993.04 m. (**h**) Off-white massive siltstone and dark-gray mudstone separated by white dotted lines, Well Ta103 at 1837.18 m. (**i**) Gray siltstone with plenty of grayish-green mud clasts (usually less than 1 cm in diameter), Well W19 at 1709.11 m. Crb-Current ripple cross-bedding. Mc-mud clast.

commonly occurs at the top of sandstone (Fig. 5g). Boring pore-bearing silty mudstone is less common. Compared with FA2 and FA3, the thin sand interlayer within mudstone is relatively less developed, while thick sandy deposits, especially fine sandstone including FStw, FSp, FSm and FSmc are more developed (Fig. 7a, d, e, f). In addition, purplish-red mud clasts and argillaceous deposits within sandstone layers are common (Figs. 6e and 7e), as well as the erosion surface (Fig. 4d). The diameter of mud clast sometimes reaches 2 cm (Fig. 7e). Furthermore, thick sandy sediments with developed erosion surfaces, parallel bedding, and other cross-bedding exhibit an upward-fining succession, and the thickness of sandy sediments may reach 10 m (Fig. 4d). Meanwhile, the lower sandy deposits and the upper argillaceous deposits in FA4 usually have an approximately equal thickness, showing a dual sedimentary texture succession (Fig. 4d). Based on the analysis of core observation and logging data, FA4 is locally distributed in the southeastern part of the study area and mainly occurred at the bottom of K_2q^4 (Sq1).

4.3.4.2. Interpretation. FA4 is interpreted as meandering river deposits characterized by dual-texture succession, widely developed purplish-red deposits, and thick sandstone (Bridge, 1993; Mail

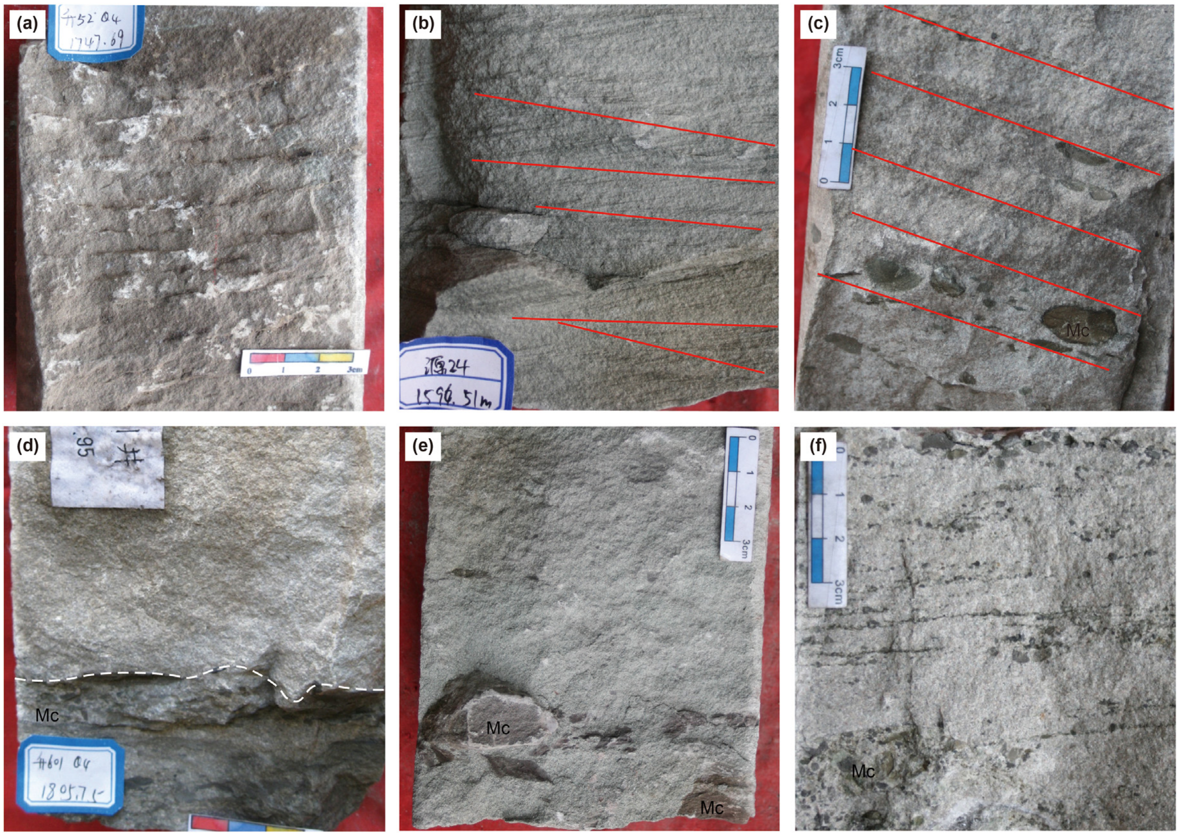

Fig. 7. Core photographs showing sedimentary characteristics of fine sandstone in K_2q^4. (**a**) Oil-immersed fine sandstone with trough cross-bedding, Well Sh52 at 1747.69 m. (**b**) Gray fine sandstone with wedge cross-bedding, Well Y24 at 1596.51 m. (**c**) Off-white parallel-bedded fine sandstone with bedding mud clasts, Well Y155 at 1696.24 m. (**d**) Off-white massive fine sandstone. The white dotted line indicates source base accompanied with grayish-green mud clasts, Well Sh601 at 1805.75 m. (**e**) Light gray massive fine sandstone with purplish-red mud clasts, Well Zh412 at 1865.24 m. (**f**) Off-white fine sandstone with plenty of interbedded mud clasts, Well Y24 at 1608.12 m. Mc-mud clast.

et al., 1996; Ghazi and Mountney, 2009; Zhu et al., 2012; Lv and Chen, 2014; Cai et al., 2016; Deng et al., 2019). Widely developed purplish-red mudstone formed in fluvial plain indicates oxidation conditions (Zhu et al., 2012; Zhang et al., 2017, 2018). Less developed gray to grayish-green mudstone is deposited in a fluvial lake. More caliche nodules in deposits are indicative of a dry and evaporitic environment (Wang et al., 2013). Thick sandstone with plenty of erosion surfaces, and mud clasts represent higher-energy channel deposits and multiple flooding activities, suggesting better stability of channels in a meandering river compared with that in deltas. Frequent occurrence of fine sandstone with coarse mud clasts in FA4 indicates a shorter distance to provenance, and the purplish-red mud clasts and argillaceous deposits in sandstone are likely originated from channel banks by erosion (Ghazi and Mountney, 2009).

4.4. Sedimentary succession and evolution

Based on the analysis of lithofacies and logging data, the facies assemblages within the K_2q^4 are mainly composed of FA3 and FA2 (Fig. 8). FA1 occurring at the top of K_2q^4 is only distributed in the western part of the study area, while FA4 appearing at the bottom of K_2q^4 is locally developed in the southern part (Fig. 9). This distribution pattern suggests that the K_2q^4 in the study area is dominated by deltaic deposits. Meanwhile, the occurrence of caliche nodules and shells in the FA1 and FA2 within the whole study area (more than 10,000 km^2) is indicative of a shallow water environment and frequent lake level fluctuations, which can also be demonstrated by the widely distributed purplish-red mudstone and frequent alternations of mudstones of different colors (Figs. 8 and 9). The K_2q^4 with relatively stable thickness and widely distributed sandstone indicate that the sedimentary environment of K_2q^4 was similar in the whole study area, and the sandstones with multiple erosion surfaces and different beddings resulted from channel deposits (Fig. 9). In addition, previous researches demonstrated that the study area experienced a stable subsidence stage and has a gentle slope on paleogeomorphology (less than 1°) during the sedimentary period of K_2q^4 (Zhu et al., 2012; Cai et al., 2016), which are favorable conditions for the formation of shallow water delta. Therefore, the above sedimentary characteristics and background suggest that the sedimentary environment of K_2q^4 in the Sanzhao depression should be dominated by shallow-water delta.

According to the lithological succession, it can be found that the lithofacies assemblages in K_2q^4 were gradually changed from FA4 to FA1 from the bottom to the top. Generally, the change from FA3 to FA2 is due to the small extent distribution of FA1 and FA4 (Figs. 8 and 9). The color of sediments gradually changes upward from purplish-red to grayish-green. In addition, the thickness of channel sandstone and the content of caliche nodules decrease upward, while the presence of pyrite in the mudstone increases (Fig. 8). These characteristics indicate that the environment of K_2q^4 gradually changed from oxidizing to reducing conditions and experienced a long-term lake level rise. In order to illustrate the depositional environment of K_2q^4 and its evolution, the simplified geological maps of sedimentary environments within the fourth-order sequence framework are compiled by the facies analysis of single wells.

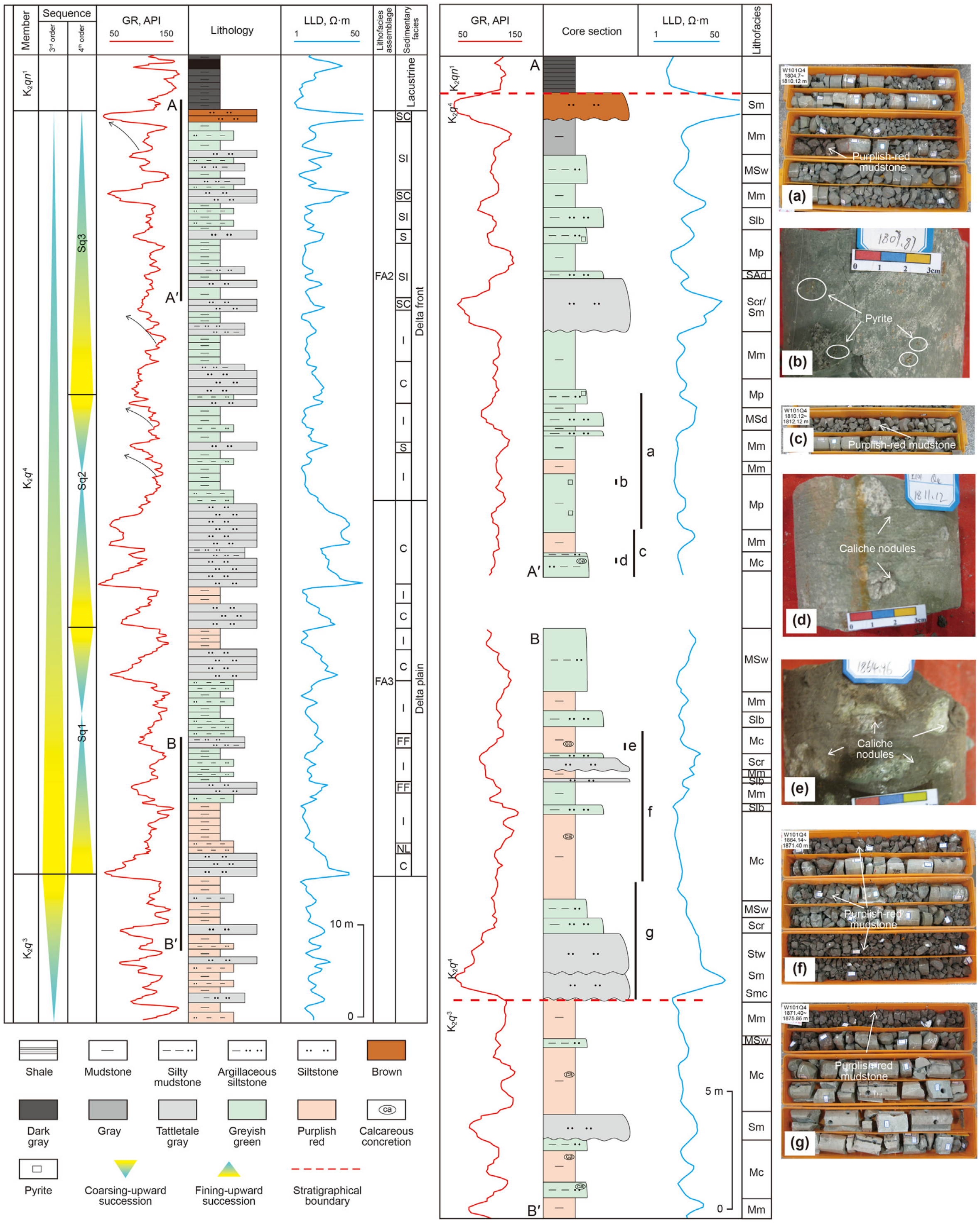

Fig. 8. Logging profile and core sections with photographs showing the lithologic features of K_2q^4 in Well W101. The locations of core sections and core photographs are marked in the pictures. (**a**) Lithological succession from 1804.70 to 1810.12 m, showing thin purplish-red mudstone and oil immersed sandstone; (**b**) Grayish-green mudstone with pyrite; (**c**) Lithological succession from 1810.12 to 1812.12 m; (**d**) Grayish-green mudstone with caliche nodules; (**e**) Purplish-red mudstone with caliche nodules; (**f**) Lithological succession from 1864.14 to 1871.40 m, showing frequent occurrence of purplish-red mudstone; (**g**) Lithological succession from 1871.40 to 1875.86 m, showing channel deposits. The abbreviation for sedimentary environment interpretation: SC-Subaqueous channel deposits; S-Sheet sand; SI-Subaqueous interchannel deposits; C-Channel deposits; I-Interchannel deposits; FF- Flood fan; NL-Natural levee.

The Sq1 within the study area mainly consists of FA3 characterized by the alternation of purplish-red and grayish-green mudstone, which is indicative of a shallow-water delta plain (Figs. 8 and 9). Meandering river deposits with dual texture succession are locally distributed in the southern parts of the study area, and the delta front characterized by grayish-green mudstone and thin sandstone are locally distributed in the west. Channel deposits with low gamma value and large thickness are widely developed in this sequence, especially in the southern part of the study area (Figs. 9 and 10). The Sq2 in the study area is mainly composed of FA3 and FA2. The increased gray and grayish-green mudstone and decreased purplish-red deposits indicate that the sedimentary environment of Sq2 changes into a reducing condition gradually, and sedimentary water depth increases with time (Fig. 8). Compared with Sq1, the shallow-water delta front deposits in this sequence increase remarkably, while delta plain deposits shrink, and meandering river deposits are not developed in the study area. Channel deposits with a smaller thickness are still widely distributed throughout the sequence (Figs. 9 and 10). The Sq3 is dominated by shallow-water delta front deposits (FA2), in which gray and grayish-green mudstones are widely distributed (Fig. 8). Shallow-water lacustrine deposits and delta plain are locally developed in the western and eastern parts of the study area, respectively (Fig. 10). It should be noted that thin purplish-red mudstone and plenty of caliche nodules in grayish-green mudstone formed under evaporated environment can be easily found in Sq3 (Figs. 8 and 9), although they show a decrease in numbers and scale. In addition, thin channel deposits in this sequence are still widely developed, even at the top of Sq3 (Figs. 8 and 10), and some sheet sand deposits can also be found (Fig. 9). These features indicate that during the sedimentary stage of Sq3, there are multiple large-scale lake level fluctuations despite the long-term lake level rise.

Therefore, according to the sedimentary succession and environment evolution, it can be found that the study area experiences a long-term lake level rise and multiple lake level fluctuations during the sedimentary stage of K_2q^4. The sedimentary environments of K_2q^4 are dominated by retrograding shallow-water delta, and channel deposits are widely distributed despite thinning upward (Figs. 9 and 10).

5. Discussions

5.1. Evidence for frequent lake level fluctuation

In previous studies, the bottom boundary of K_2q^4 in the Songliao Basin is interpreted as the regionally exposed surface marked by purplish-red paleosol layer, and the top boundary is regarded as a maximum flooding surface marked by K_2qn^1 oil shale (Feng et al., 2010; Pan et al., 2012; Zhu et al. 2012, 2017b; Wang et al., 2013; Cai et al., 2016; Deng et al., 2019) (Figs. 2b, 8 and 11). Based on lithological succession, there is no doubt that the lake level in the study area shows a long-term increase from the bottom to the top of K_2q^4, in which the color of mudstone changes from purplish-red to grayish-green, and channel deposits thinning upward (Cai et al., 2016; Meng et al., 2016) (Figs. 8 and 9). However, previous researchers indicate that the rise of lake level is generally unstable in a sedimentary basin, especially in a large basin with a gentle slope, and much attention should be paid to lake level fluctuations due to its significant influence on deposits (Lou et al., 1999; Cai et al., 2011; Zeng et al., 2017).

The core and debris logs from almost all single wells in the study area show that the occurrences of purplish-red mudstone and grayish-green mudstone in K_2q^4 are alternated frequently, despite their macro-regularity from the bottom to the top (Figs. 8 and 9). Purplish-red mudstone formed under oxidizing environment can develop in the top of K_2q^4 within thick grayish-green mudstone formed under a humid and reducing environment (Figs. 8, 9 and 11). Similarly, the thin grayish-green mudstone can also develop in thick purplish-red mudstone, and thin sandstone can develop at the top of K_2q^4 covered by black oil shale (Figs. 8 and 9). Although, the occurrences of caliche nodules and purplish-red mudstone

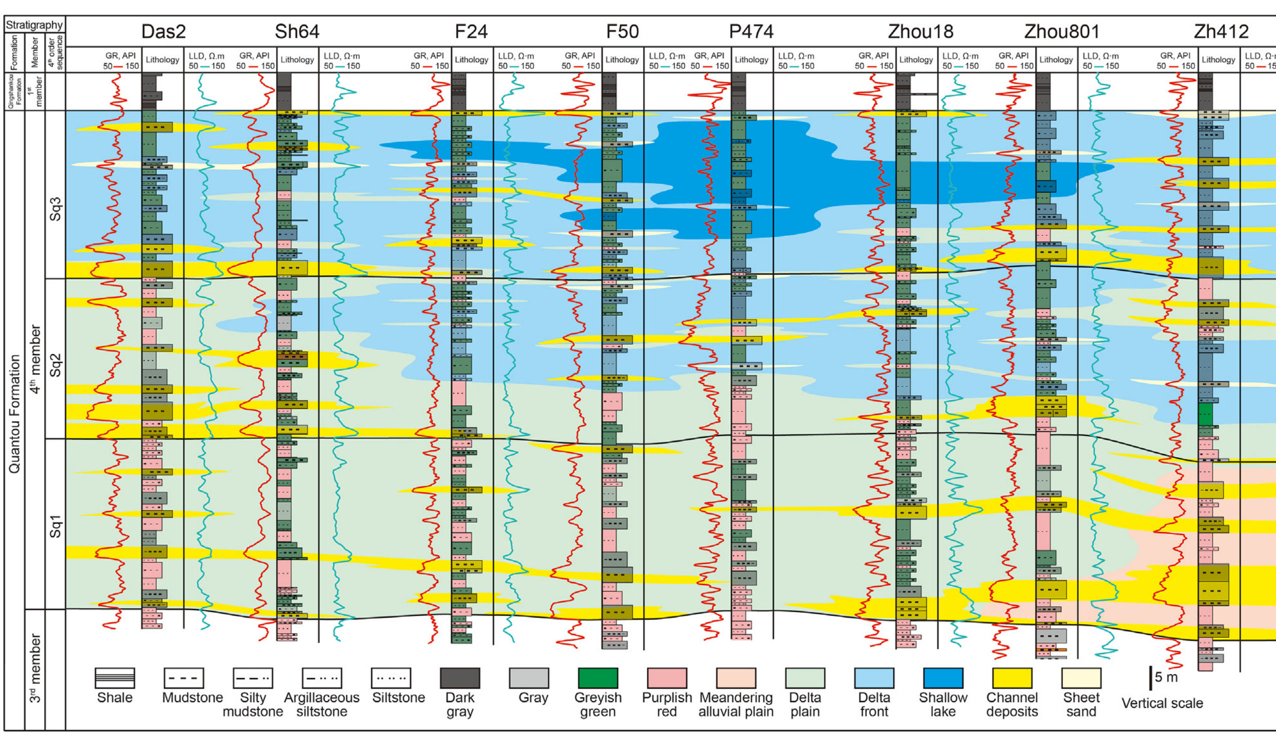

Fig. 9. Correlations of eight wells showing lithological associations and depositional environments of K_2q^4 within the Sanzhao depression (The profile location has been shown in Fig. 1 BB′).

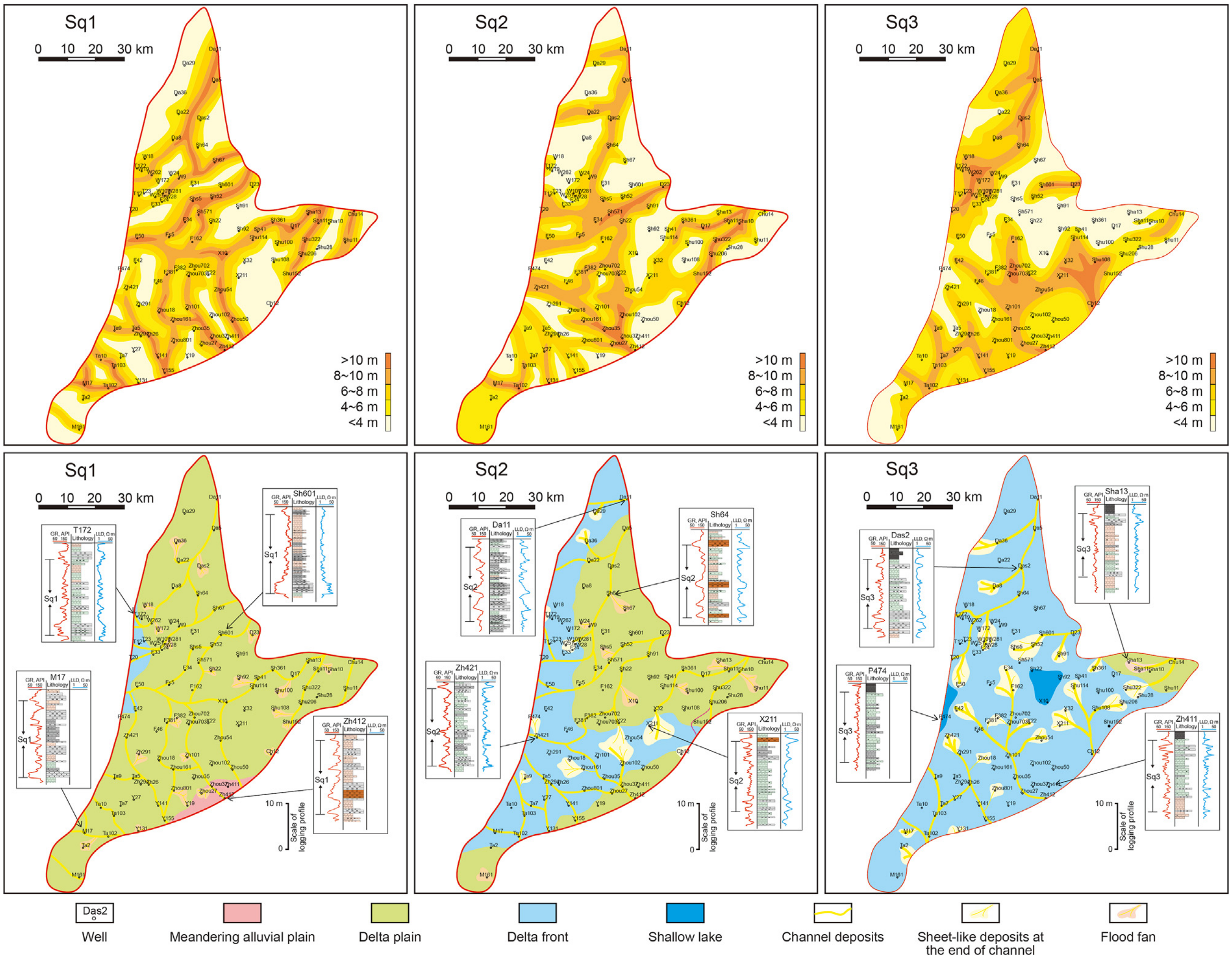

Fig. 10. Sandstone distribution and sedimentary facies of the three fourth-order sequences in K_2q^4 within the Sanzhao depression, Songliao Basin. The data are obtained from cores, logging, and boreholes.

have opposite vertical variations to pyrite particles and grayish-green mudstone, caliche nodules formed in evaporated environments are very common in K_2q^4, even in FA1 (Fig. 4a and b and 8). In addition, gamma log curves and lithological associations show that there are many small coarsening-upward sequences in the K_2q^4 (Fig. 8). These features indicate that during the sedimentary stage of K_2q^4, the lake level rise in the study area is not stable, which may experience multiple fluctuations. Caliche nodules and thin purplish-red mudstone within grayish-green mudstone are the deposits formed during short-time lake level decline.

Moreover, the geochemical data of K_2q^4 from Well Sheng 41 indicate that the CIA values slightly increases upward showing that the paleoclimate changed from semiarid to semihumid, and a clear fluctuation of CIA value is also shown in Fig. 11. Similarly, the geochemical proxy Fe/Mn, as an effective indicator of water depth in a lake (Tian et al., 2006), also fluctuates obviously in the K_2q^4 (Fig. 11). These features show that the paleoclimate and the sedimentary environment of K_2q^4 in the study area are not stable, and the lake level may frequently fluctuate due to climate change despite long-term lake level rise (Zhu et al., 2012; Wang et al., 2013; Zhang et al., 2018; Jones et al., 2018; Deng et al., 2019). The gentle slope of basin floors also provides advantageous conditions for frequently and large-scale lake level fluctuations (Li et al., 2014; Xin et al., 2019; Zhu et al., 2017b; Zeng et al., 2017; Wang et al., 2020), which can also be used to interpret the wide distribution of caliche nodules and thin purplish-red mudstone in the grayish-green mudstone of FA1 within the whole study area.

Many examples of large-scale and frequent lake level fluctuations have been found in modern shallow lakes (Leeben et al., 2013; Gałka and Apolinarska, 2014; Huang et al., 2014; You et al., 2015; Deng et al., 2015; Zhang et al., 2016; Ning et al., 2018). The Poyang Lake located in Jiangxi Province, central China, is a typical case (Fig. 12a and b), which is mainly supplied by the Gan River and is identified as a shallow lake with a gently slope base lower than one degree (<1°) (Zhang et al., 2012; Deng et al., 2015). Previous researches indicate that the sedimentary environment of Poyang Lake is dominated by shallow-water delta to shallow lacustrine systems, and the lake level commonly fluctuates caused by climate changes (Zhang et al., 2012; Huang et al., 2014; Deng et al., 2015; Zhang et al., 2016; Ning et al., 2018). For example, in 2013, the lake surface areas on February 1, 2013 and May 22, 2013 were clearly different with the coming of the rainy season (Fig. 12c and d). Moreover, the hydrometric data from 1990 to 2009 show that the lake level in Poyang Lake fluctuated frequently, as well as the lake area (Fig. 12e and f). In addition, according to isotope dating and lithological investigation of Poyang Lake sediments, Liang et al. (2016) pointed out that during the past 6000 years, the color of clay in the Poyang formation exhibits alternations of steel gray and

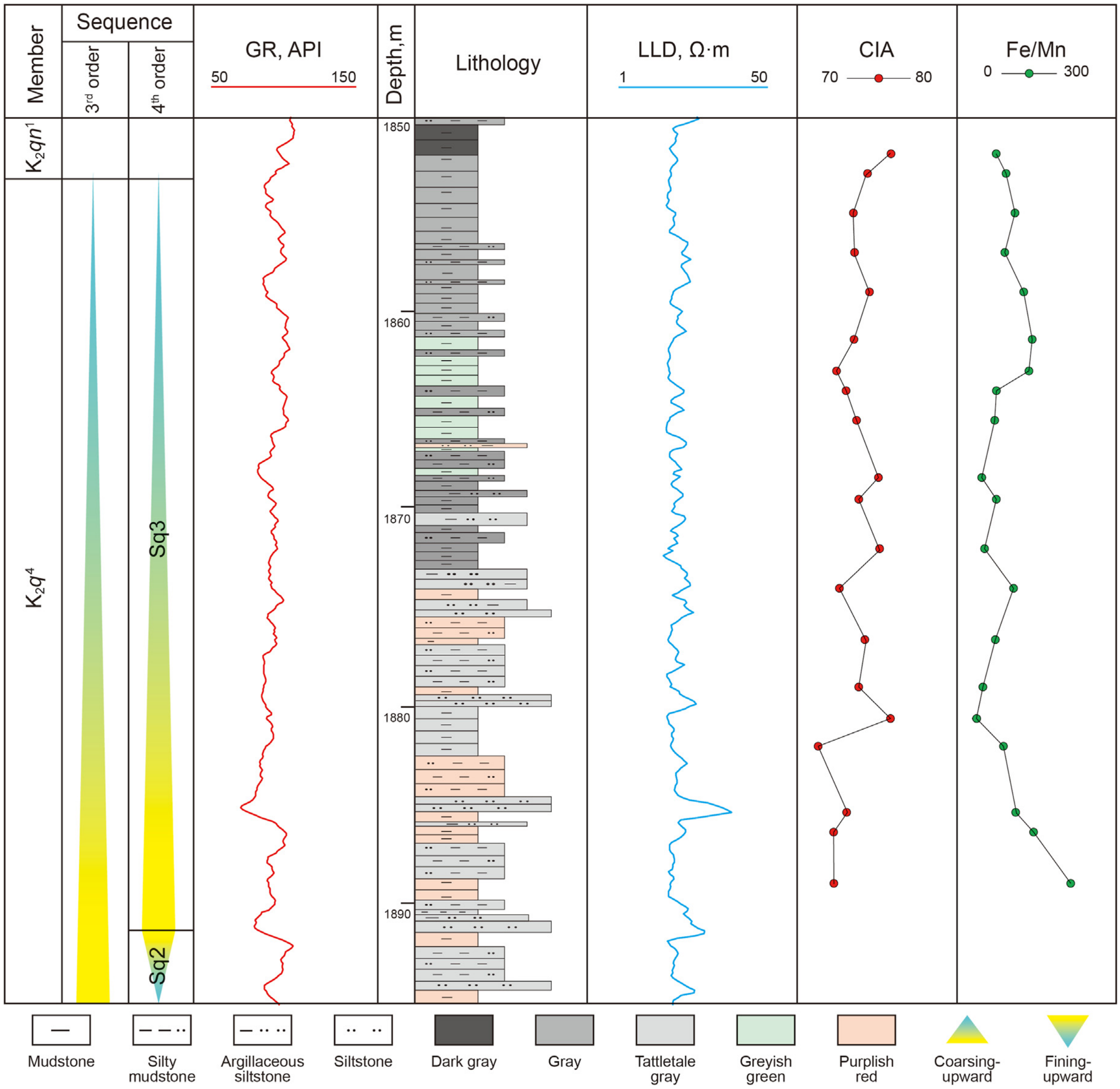

Fig. 11. CIA values and Fe/Mn ratios of mudstone from K_2q^4 in Well Sheng 41.

yellowish brown with lake level fluctuation, and thin channel sandstone can be migrated quickly to lake center when lake level decrease (Ma et al., 2003; Huang et al., 2014; Zhang et al., 2016; Liang et al., 2016). Although the lake level changes in the period of K_2q^4 in the Songliao Basin may be incompletely similar with that in the Poyang Lake, this example indicates that lake level in a shallow lake can be fluctuated frequently by the influence of climate change, and the small lake level variations will lead to remarkable changes in lake surface area and deposits (Fig. 12f).

5.2. Depositional model

Based on the above analysis of lithological succession, sedimentary facies, and geological background, we infer that the study area experience frequent lake level fluctuations during the depositional stage of K_2q^4 resulting from unstable climate change, and despite the long-term lake level rise, the K_2q^4 in the study area should be the result of a retrograding shallow-water delta deposition under two different sedimentary conditions: arid paleoclimate with a low lake level, and humid paleoclimate with a high lake level (Fig. 13). In order to present the sedimentary process of K_2q^4, we try to establish two depositional models for a basin with a gentle basement under different sedimentary conditions.

Under relatively arid conditions, the lake level and area decrease rapidly and most areas are exposed due to insufficient water supply. By the enhanced evaporation and oxidation, pyrite in mudstone is very rare, while purplish-red mudstone is widely distributed, as well as the caliche-nodule bearing mudstone formed in alluvial plain and restricted alluvial lake (Zhu et al., 2012; Zhang et al., 2018). Channel sandstone containing plenty of purplish-red mud clasts and argillaceous matrix are more common in delta plain and meandering river environments (Fig. 13a). In this model, shallow lacustrine facies may disappear and the delta front area shrinks significantly, meandering river near the source area develops gradually. Channel deposits will migrate towards the lake center with continuous lake level decline, leading to widely distributed channel sandstone. The thickness of widely distributed channel sandstone is closely related to the duration time of arid paleoclimate with low lake water level and the subsequent reformation by enhanced lake wave under humid climate conditions.

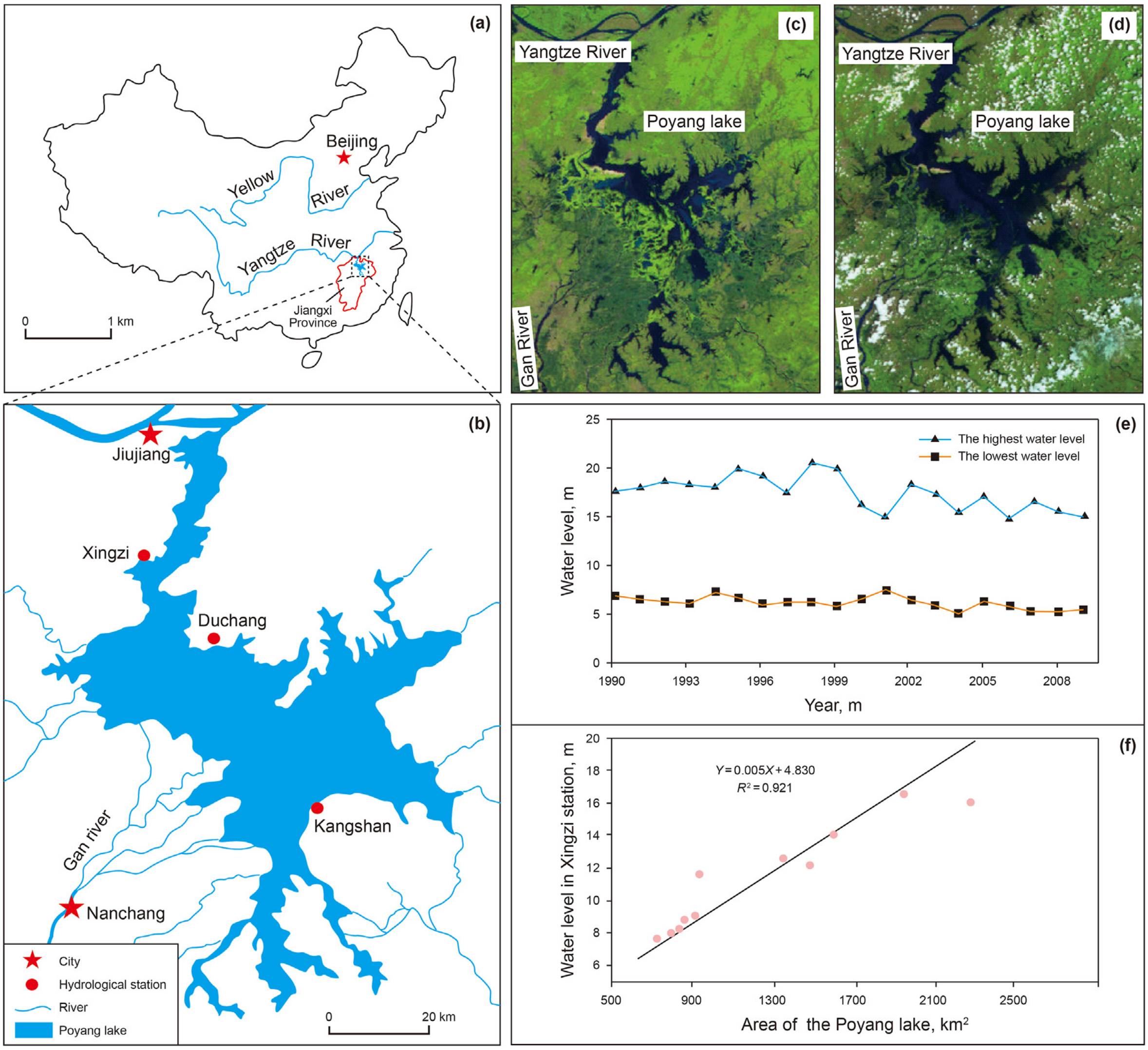

Fig. 12. Location and lake level fluctuations of Poyang Lake. (**a**) Location of Poyang Lake in China. (**b**) Area of Poyang Lake and its river systems. (**c**) Satellite image on February 1, 2013 shows the water area of Poyang Lake. (**d**) Satellite image on May 22, 2013 shows the water area of Poyang Lake. (**e**) Lake level fluctuations in Poyang Lake from 1990 to 2009 (data from Deng et al., 2015). (**f**) Relationship between water level and water area of the Poyang Lake (data from Zhang et al., 2012).

For relatively humid climate conditions, the lake area can be increased significantly with a rising lake level caused by enough water supply (Postma, 2001; Wang et al., 2013; Zhu et al., 2017b; Xin et al., 2019) (Fig. 13b). In this model, the sedimentary environment gradually becomes more reducing, lacustrine argillaceous sediments including pyrite-bearing mudstone are common, while caliche-nodule bearing mudstone is rare. The occurrence of fine sandstone and purplish-red mudstone decrease gradually. Some mud clasts that occurred at the bottom of the channel deposits are dominated by grayish-green and gray colors. By the intensifying resistance of lake water, channels in delta plain bifurcate frequently. Sandstone developed at the end of subaqueous channels can be reformed to sheet-like sand by enhanced lake wave with gradual lake level rise, leading to a small thickness of subaqueous channel sandstone. Vertically, it can be found that the scale of channel deposits in this model decreases gradually and sandstone in the lake center are usually less developed (Fig. 13b).

For the K_2q^4 in the study area, the intermittent occurrence of purplish-red mudstone and CIA values indicate that the climate changes (from semi-arid to semi-humid) during the depositional stage of K_2q^4 is not stable (Figs. 8 and 11). From the bottom to the top, the decrease of the thickness of caliche-nodule bearing mudstone and purplish-red mudstone shows a shorter duration time of semi-arid climate with low lake level and a longer duration time of semi-humid climate with high lake level. As the above presented models, low lake level will lead to channel deposits migrating towards the lake center, while high lake level will lead to the migration of channel deposits towards the land and the reformation of sand bodies developed at the end of the subaqueous channels. Therefore, according to the sedimentary characteristics of K_2q^4, it can be inferred that with lake level fluctuations and unstable climate changes, the two sedimentary models shown above alternate frequently in the study area (Fig. 13c), despite the long-term lake level rise during the depositional stage of K_2q^4.

5.3. *Formation of widespread sandstone and implications for oil & gas exploration*

The distribution of sandstone in delta deposits is a primary concern for oil and gas exploration (Olariu and Bhattacharya, 2006; Zou et al., 2006; Zhu et al. 2008, 2012, 2013a, 2013b; Wang et al., 2012; Zhao et al., 2011b; Liu et al., 2015; Cai et al., 2016; Wang

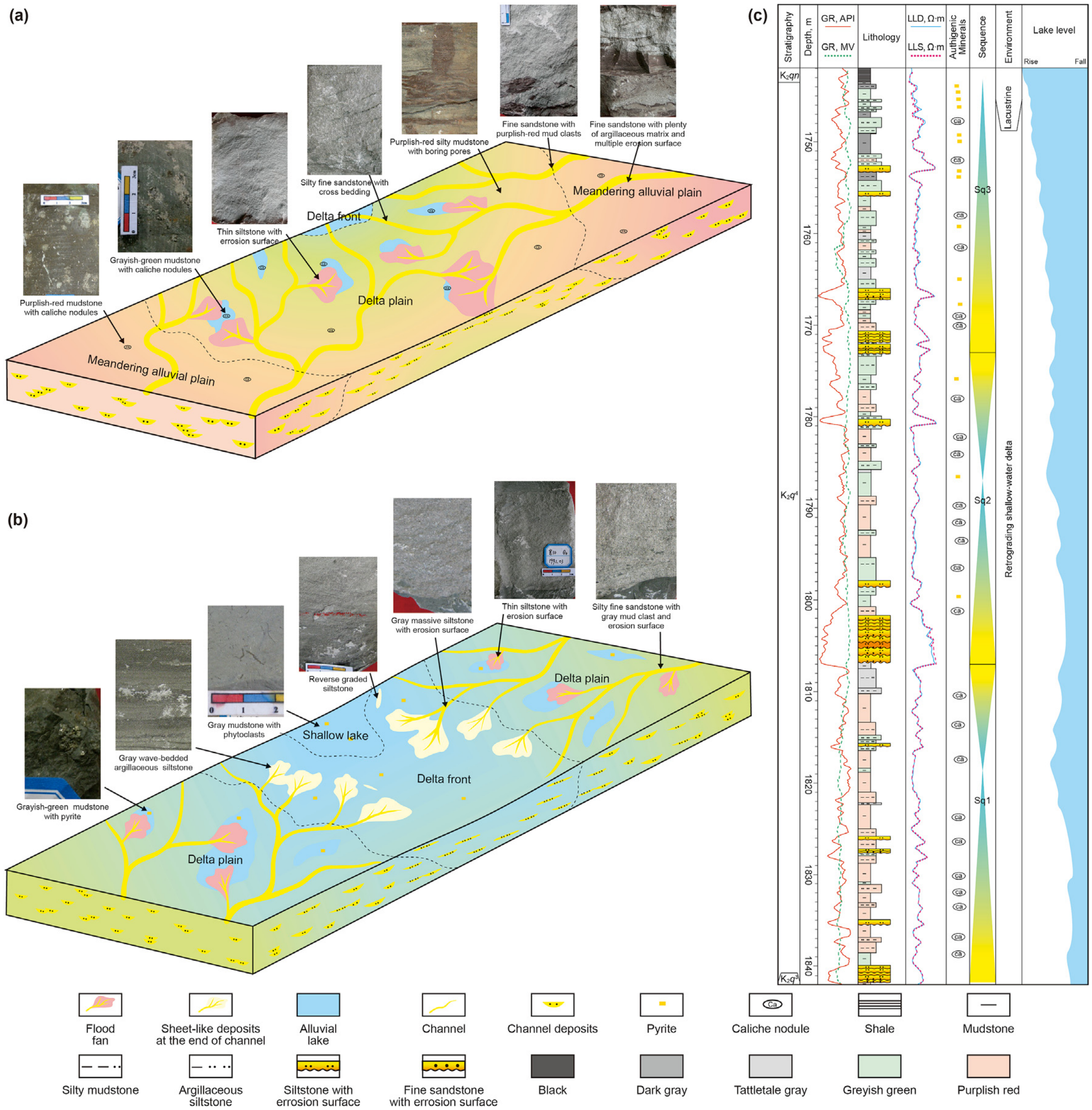

Fig. 13. Depositional models for the retrograding shallow-water delta of K_2q^4 in the Sanzhao depression, Songliao Basin. Core photographs showing typical lithological characteristics under different sedimentary conditions. (**a**) Depositional model of shallow-water delta with low lake level resulting from arid paleoclimate. (**b**) Depositional model of shallow-water delta with high lake level resulting from humid paleoclimate. (**c**) Simplified sedimentary profile (Well Zhao 401) showing retrograding shallow-water delta deposits of K_2q^4 in the study area.

et al., 2019; Dou et al., 2020). Channel sandstone is considered as the main part of sand bodies in a shallow-water delta (Lou et al., 2004; Cai et al., 2011; Edmonds et al., 2011; Chen et al., 2015; Zhu et al., 2017b; Zhang et al., 2017, 2018; Tian et al., 2019; Wang et al., 2019; Wang et al., 2020). For the K_2q^4 in the study area, although the thickness of successive channel sandstone was gradually thinning upward, the channel sandstone is still widely developed in the whole study area (Fig. 10), even at the top of K_2q^4 (Figs. 8, 9 and 14). The frequent migration of channels is usually considered as an important factor for the formation mechanism of widespread channel sandstone in shallow-water delta (Rahman et al., 2014; Zhu et al., 2012, 2013b, 2017b; Liu et al., 2015; Zhang et al., 2017; Xin et al., 2019; Tian et al., 2019; Deng et al., 2019). However, during the depositional stage of K_2q^4, the lake level in the study area shows a long-term rising trend with a paleoclimate changed from semi-arid to semi-humid (Wu et al., 2009; Wang et al., 2013; Zhao et al., 2014; Zhu et al., 2017b; Jones et al., 2018; Yang, 2018), and the sedimentary environment of K_2q^4 in the study area was dominated by a retrograding shallow-water delta. By the influence of lake level rise, most underwater distributary channels may not extend tens of kilometers (Reading, 1996; Cai et al., 2016; Zhang et al., 2018). Therefore, the migration of underwater distributary channels cannot be applied to explain the widely distributed channel sandstone directly, especially the channel sandstone near the lake center and covered by black oil shale (Figs. 9, 10 and 14). Based on the lithological succession and sedimentary background of K_2q^4, we infer that frequent lake level fluctuations caused by unstable paleoclimate changes should be the ultimate controlling factor for the widely distributed channel sandstone in the study area.

As we know, the paleoclimate of the study area changed from semi-arid to semi-humid gradually during the depositional stage of K_2q^4, but the climate changes were not stable (Wu et al., 2009; Wang et al., 2013; Zhao et al., 2014; Jones et al., 2018; Yang, 2018).

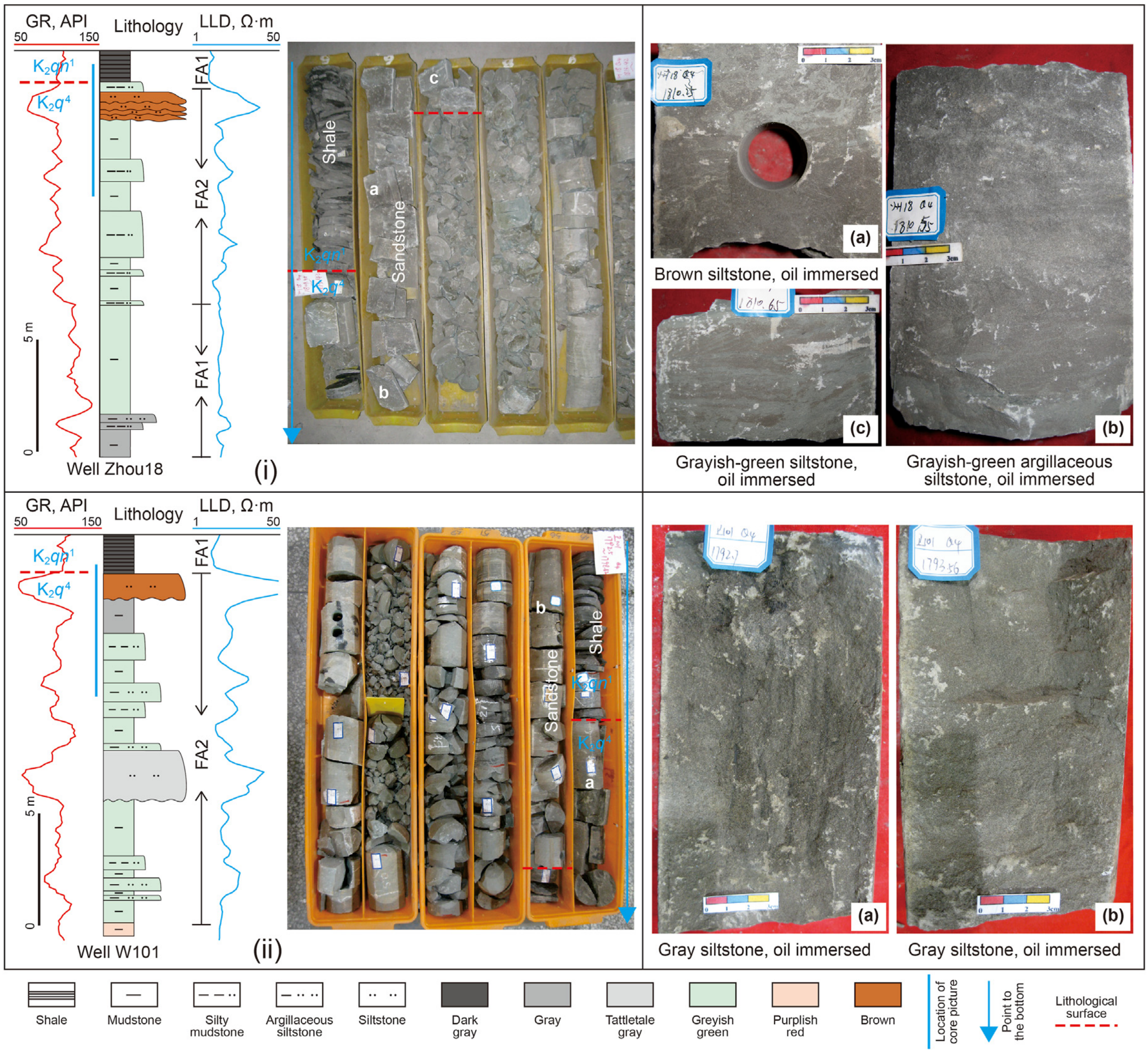

Fig. 14. Oil-immersed channel sandstone distributed at the top of K_2q^4, covered by oil shale of K_2qn^1. The locations of cores are shown in each picture.

When the paleoclimate is inclined to be semi-humid, the lake level will rise with sufficient water supply, and a slight increase of lake level will lead to a dramatic expansion of the lake area due to the gentle slope of the basin floor (Fig. 13a), just as what happened to the modern Poyang lake (Fig. 12). With gradually deepening lake water and increase of flood activity, channels of delta bifurcate frequently and sandstone deposits migrate towards land by the resistance of lake water. Meanwhile, previous channel deposits may be reformed by enhanced lake wave activity leading to gradually developed sheet-like sand (Lou et al., 1999; Cai et al., 2011; Zeng et al., 2017). On the contrary, when the paleoclimate is inclined to be semiarid, a slight decrease of lake level caused by insufficient water supply will lead to a dramatic decrease of lake area (Lou et al., 2004; Zhu et al., 2012; Cai et al., 2016) (Fig. 13b). Channels of delta migrate towards the lake center leading to widely distributed sandstone in the whole area. But with the long-term climate changed gradually from semi-arid to semi-humid, the occurrence frequency and duration of short-time semi-arid condition decrease, leading to the insufficient input of coarse deposits and the thinning of channel sandstone in the lake center. This may be why the channel sandstone deposits distributed at the top of K_2q^4 usually has a relatively small thickness. Therefore, it can be concluded that the widely developed channel sandstone in a retrograding shallow-water delta is the result of channel migration and lake level fluctuation caused by climate changes, and the duration time of relatively arid paleoclimate and lake wave reformation control the thickness of channel sandstone near lake center. In addition, according to core observations, it should be noted that almost all thin sand bodies at the top of K_2q^4, especially distributed in the lake center covered by black oil shale are oil-immersed (Fig. 14), indicating that thin channel sand layers of retrograding shallow-water delta near source rocks should be of great significance for lithological hydrocarbon exploration.

6. Conclusions

1. Four facies assemblages in the K_2q^4 are established based on detailed sedimentary facies analysis, representing various depositional environments from meandering river to shallow-water delta to shallow lacustrine systems, but the K_2q^4 is dominated by FA2 and FA3. The sedimentary succession and evolution of the K_2q^4 show that the lake level in the study area rises gradually, and the sedimentary environment is dominated by a retrograding shallow-water delta.

2. Despite the long-term increase in lake level, the grayish-green mudstone and purplish-red mudstone are developed alternatively, caliche nodules and pyrite in mudstone are homogeneously distributed, and geochemical proxy values fluctuate obviously, indicating that the lake level rise during the depositional stage of K_2q^4 was not stable but fluctuates frequently. Similar lake level changes can be found in modern lakes. The K_2q^4 should be the results of two depositional models with different lake level caused by climate changes.
3. In a retrograding shallow-water delta, the widely distributed channel sandstone are results of channel migration and lake level fluctuations triggered by climate change, and the decrease of duration of semiarid condition and enhanced lake wave activity under semihumid climate leads to upward thinning channel deposits. Due to good relationship with upper source rocks, thin channel sandstone developed at the top of a retrograding shallow-water delta sedimentary succession are commonly oil immersed. Therefore, more attention should be paid to lake level fluctuations and thin channel sandstone distribution within a retrograding shallow-water delta, and it will be of great significance for lithologic reservoir exploration.

Acknowledgements

This study was financially supported by the National Science and Technology Major Project of China (H.M.Y., grant number 2016ZX05013006-006) and Natural Science Foundation of Hubei Province of China (L.H., grant number 2020CFB745). We appreciate the constructive suggestions received from Dr. D. Gao and M.T. Li. We also thank the Exploration and Development Research Institute of Daqing Oilfield Co Ltd. for the data support. In addition, the critical and helpful comments, and suggestions from the editor and two anonymous reviewers are greatly appreciated.

References

Bridge, J.S., 1993. Description and interpretation of fluvial deposits: a critical perspective. Sedimentology 40, 801–810. https://doi.org/10.1111/j.1365-3091.1995.tb02110.x.

Cai, Q.S., Hu, M.Y., Hu, Z.G., et al., 2016. Sedimentary evolution and distribution of sand bodies of retrogradational shallow-water delta: a case study from 4th member of the Cretaceous Quantou Formation in the Lingjiang area, Songliao Basin. Oil Gas Geol. 37, 903–914. https://doi.org/10.11743/ogg20160612 (in Chinese).

Cai, Q.S., Hu, M.Y., Ngia, N.R., et al., 2017. Sequence stratigraphy, sedimentary systems and implications for hydrocarbon exploration in the northern Xujiaweizi Fault Depression, Songliao Basin, NE China. J. Petrol. Sci. Eng. 152, 471–494. https://doi.org/10.1016/j.petrol.2017.02.022.

Cai, X.Y., Zhu, R., 2011. Cretaceous sandbody characters at shallow-water lake delta front and the sedimentary dynamic process analysis in Songliao Basin, China. Acta Geol. Sin. 85, 1478–1494. https://doi.org/10.1111/j.1755-6724.2011.00600.x.

Cao, Y.C., Han, M., Wang, Y.Z., et al., 2010. Sedimentary characteristics and models of shallow-water delta deposits in the second member of the Shahejie Formation in the Chezhen Sag, the Jiyang Depression. Oil Gas Geol. 31, 576–582. https://doi.org/10.11743/ogg20100507 (in Chinese).

Chen, L., Lu, Y.C., Wu, J.Y., et al., 2015. Sedimentary Facies and Depositional Model of Shallow Water Delta Dominated by Fluvial for Chang 8 Oil-Bearing Group of Yanchang Formation in Southwestern Ordos Basin, China, vol. 22. Journal of Central South University, pp. 4749–4763. https://doi.org/10.1007/s11771-015-3027-3.

Cornel, O., Janok, P.B., 2006. Terminal distributary channels and delta front architecture of river-dominated delta systems. J. Sediment. Res. 76, 212–233. https://doi.org/10.2110/jsr.2006.026.

Deng, Q.J., Hu, M.Y., Hu, Z.G., 2019. Depositional characteristics and evolution of the shallow water deltaic channel sand bodies in Fuyu oil layer of central downwarp zone of Songliao Basin, NE China. Arabian J. Geosci. 12 (20), 1–14. https://doi.org/10.1007/s12517-019-4762-9.

Deng, Q.J., Hu, M.Y., Liu, X.D., et al., 2018. Development and characteristics of sedimentary facies and sand-bodies of the Cretaceous Fuyu oil layer within high-resolution sequence framework, Shuangcheng Block, Songliao Basin. J. Palaeogeogr. 20 (2), 311–324. https://doi.org/10.7605/gdlxb.2018.02.023 (in Chinese).

Deng, Z.M., Zhang, X., Xiao, Y., et al., 2015. Study of evolution of water level in Poyang Lake and impact factors. Engineering Journal of Wuhan University 48, 615–621. https://doi.org/10.14188/j.1671-8844.2015-05-004 (in Chinese).

Donaldson, A.C., 1974. Pennsylvanian sedimentation of central appalachians. Geological Society of America Special Papers, pp. 47–78. https://doi.org/10.1130/SPE148-p47.

Dou, L.X., Hou, J.G., Liu, Y.M., et al., 2020. Sedimentary infill of shallow water deltaic sand bodies controlled by small-scale syndepositional faults related paleogeomorphology: insights from the paleogene Shahejie formation in the Dongying depression, Bohai Bay Basin, Eastern China. Mar. Petrol. Geol. 118, 104420. https://doi.org/10.1016/j.marpetgeo.2020.104420.

Edmonds, D.A., Shaw, J.B., Mohrig, D., 2011. Topset-dominated deltas: a new model for river delta stratigraphy. Geology 39, 1175–1178. https://doi.org/10.1130/G32358.1.

Feng, W.J., Zhang, C.M., Yin, T.J., et al., 2019. Sedimentary characteristics and internal architecture of a river-dominated delta controlled by autogenic process: implications from a flume tank experiment. Petroleum Science. 2019 16 (6), 1237–1254. https://doi.org/10.1007/s12182-019-00389-x.

Feng, Z.Q., Jia, C.Z., Xie, X.N., et al., 2010. Tectonostratigraphic units and stratigraphic sequences of the nonmarine Songliao basin, northeast China. Basin Res. 22, 79–95. https://doi.org/10.1111/j.1365-2117.2009.00445.x.

Fielding, C.R., Trueman, J.D., Alexander, J., 2006. Holocene depositional history of the Burdekin River delta of northeastern Australia: a model for a low-accommodation, highstand delta. J. Sediment. Res. 76, 411–428. https://doi.org/10.2110/jsr.2006.032.

Fisk, H.N., Kolb, C.R., McFarlan, E.J., et al., 1954. Sedimentary framework of the modern Mississippi Delta. J. Sediment. Res. 24 (2), 76–99. https://doi.org/10.1306/D4269661-2B26-11D7-8648000102C1865D.

Folk, R.L., 1974. Petrology of sedimentary rocks. Hemphill. Austin, Texas, p. 182. https://doi.org/10.1007/978-94-011-9640-6.

Gałka, M., Apolinarska, K., 2014. Climate change, vegetation development, and lake level fluctuations in Lake Purwin (NE Poland) during the last 8600 cal. BP based on a high-resolution plant macrofossil record and stable isotope data ($\delta\ ^{13}C$ and $\delta\ ^{18}O$). Quat. Int. S328–329, 213–225. https://doi.org/10.1016/j.quaint.2013.12.030.

Ghazi, S., Mountney, N.P., 2009. Facies and architectural element analysis of a meandering fluvial succession: the Permian Warchha Sandstone, Salt Range, Pakistan. Sediment. Geol. 221, 99–126. https://doi.org/10.1016/j.sedgeo.2009.08.002.

Gilbert, G.K., 1885. The topographic features of lake shores. U. S. Geol. Surv. Annu. Rep. 5, 69–123. https://doi.org/10.1038/034269a0.

Heckel, P.H., 1972. Possible inorganic origin for stromatactis in calcilutite mounds in the Tully Limestone, Devonian of New York. J. Sediment. Petrol. 42, 7–18. https://doi.org/10.1306/74D72478-2B21-11D7-8648000102C1865D.

Horne, J.C., Ferm, J.C., Caruccio, F.T., et al., 1978. Depositional models in coal exploration and mine planning in Appalachian Region. AAPG (Am. Assoc. Pet. Geol.) Bull. 62, 2379–2411. https://doi.org/10.1007/BF02634580.

Hoy, R.G., Ridgway, K.D., 2003. Sedimentology and sequence stratigraphy of fan-delta and river-delta deposystems, Pennsylvanian Minturn Formation, Colorado. AAPG (Am. Assoc. Pet. Geol.) Bull. 87, 1169–1191. https://doi.org/10.1306/03110300127.

Hu, M.Y., Sun, C.Y., Xue, D., Zhang, H.J., 2015. Study of high-resolution sequence stratigraphy of quan 4th member, Sanzhao area in the northern Songliao Basin. Geoscience 29, 765–776. https://doi.org/10.3969/j.issn.1000-8527.2015.04.006 (in Chinese).

Huang, X., Liu, K.Y., Zou, C.N., 2014. Forward stratigraphic modelling of the shallow-water delta system in the Poyang Lake, southern China. J. Geochem. Explor. 144, 74–83. https://doi.org/10.1016/j.gexplo.2014.01.019.

Jones, M.M., Ibarra, D.E., Gao, Y., et al., 2018. Evaluating Late Cretaceous OAEs and the influence of marine incursions on organic carbon burial in an expansive East Asian paleo-lake. Earth Planet Sci. Lett. 484, 41–52. https://doi.org/10.1016/j.epsl.2017.11.046.

Lai, H.F., Qin, Z., Wang, H.J., et al., 2017. Development pattern of shallow-water delta and sandbodies under control of high-frequency base-level cycles: A case study of the Cretaceous Quantou Formation in Fuyu Oilfield, Songliao Basin. J. Palaeogeogr. 19 (4), 609–622. https://doi.org/10.7605/gdlxb.2017.04.047.

Leckie, D.A., Wallace-Dudley, K.E., Vanbeselaere, N.A., et al., 2004. Sedimentation in a low-accommodation setting: non-marine (cretaceous) mannville and marine (Jurassic) Ellis groups, manyberries field, southeastern Alberta. AAPG (Am. Assoc. Pet. Geol.) Bull. 88, 1391–1418. https://doi.org/10.1306/05120403131.

Lee, K., McMechan, G.A., Gani, M.R., et al., 2007. 3-D architecture and sequence stratigraphic evolution of a forced regressive top-truncated mixed-influenced delta, Cretaceous Wall Greek sandstone, Wyoming, USA. J. Sediment. Res. 77, 303–323. https://doi.org/10.2110/jsr.2007.031.

Leeben, A., Freiberg, R., Tõnno, I., et al., 2013. A comparison of the palaeolimnology of Peipsi and Võrtsjärv: connected shallow lakes in north-eastern Europe for the twentieth century, especially in relation to eutrophication progression and water-level fluctuations. Hydrobiologia 710, 227–240. https://doi.org/10.1007/s10750-012-1209-7.

Lemons, D.R., Chan, M.A., 1999. Faciès architecture and sequence stratigraphy of fine-grained lacustrine deltas along the eastern margin of late pleistocene lake bonneville, Northern Utah and Southern Idaho. AAPG (Am. Assoc. Pet. Geol.) Bull. 83, 635–665. https://doi.org/10.1306/00AA9C14-1730-11D7-8645000102C1865D.

Li, D., Dong, C.M., Lin, C.Y., et al., 2013. Control factors on tight sandstone reservoirs below source rocks in the Rangzijing slope zone of southern Songliao Basin,

East China. Petrol. Explor. Dev. 40, 692–700. https://doi.org/10.1016/S1876-3804(13)60099-3.
Li, J.P., Liu, Hao, Niu, C.M., et al., 2014. Evolution regularity of the Neogene shallow water delta in the Laibei area Bohai Bay Basin, northern China. J. Palaeogeogr. 3, 257–269. https://doi.org/10.3724/SP.J.1261.2014.00055.
Li, S.Q., Chen, F.K., Siebel, W., et al., 2012. Late Mesozoic tectonic evolution of the Songliao Basin, NE China: evidence from detrital zircon ages and Sr-Nd isotopes. Gondwana Res. 22, 943–955. https://doi.org/10.1016/j.gr.2012.04.002.
Liang, Y.H., Shi, Y.M., Xu, L., et al., 2016. A study of comparative sedimentology on fuyu Oilfield. Sci. Technol. Eng. 16 (14), 115–122. https://doi.org/10.3969/j.issn.1671-1815.2016.14.021 (in Chinese).
Li, Y.P., Yu, K., Jiang, Y.J., et al., 2007. A new Explanation for the stratigraphical sequence of quan 4th member of the fuyu oil layer in the Songliao Basin. Periodical of Ocean University of China 37, 977–982. https://doi.org/10.1631/jzus.2007.B0900 (in Chinese).
Lin, X.X., Hou, Z.J., 2014. A quantitative analysis research on relative lacustrine level changes in the lower cretaceous fuyu reservoir in the Songliao Basin. J. Stratigr. 38, 170–180. https://doi.org/10.19839/j.cnki.dcxzz.2014.02.005 (in Chinese).
Liu, Z.B., Lv, Y.F., Fu, X.F., et al., 2009. Sedimentary characteristics and hydrocarbon accumulation model of Fuyu reservoir in the Sanzhao Depression. J. Jilin Univ. (Earth Sci. Ed.) 39, 998–1006. https://doi.org/10.3969/j.issn.1671-5888.2009.06.006 (in Chinese).
Liu, Z.L., Zhu, X.M., Li, F.J., et al., 2015. Formation conditions and sedimentary characteristics of a triassic shallow water braided delta in the Yanchang formation, Southwest Ordos basin, China. PLoS One 10, 1–19. https://doi.org/10.1371/journal.pone.0119704.
Lou, Z.H., Lan, X., Lu, Q.M., et al., 1999. Controls of the topography, climate, and lake level fluctuation on the depositional environment of a shallow-water delta: a case study of the Cretaceous Putaohua reservoir. Acta Geol. Sin. 73, 83–92. https://doi.org/10.1111/j.1755-6724.1999.tb00819.x (in Chineset).
Lou, Z.H., Yuan, D., Jin, A.M., 2004. Types, characteristics of sandbodies in shallow-water delta front and sedimentary models in northern Songliao Basin, China. J. Zhejiang Univ. (Sci. Ed.) 31, 211–215. https://doi.org/10.1007/BF02911025 (in Chinese).
Lv, D.W., Chen, J.T., 2014. Depositional environments and sequence stratigraphy of the Late Carboniferous–Early Permian coal-bearing successions (Shandong Province, China): sequence development in an epicontinental basin. J. Asian Earth Sci. 79, 16–30. https://doi.org/10.1016/j.jseaes.2013.09.003.
Ma, Z.X., Jiang, Y.Z., Wei, Y., Li, J.H., Li, C.A., 2003. Reversion and characters of the poyanghu formation (Quaternary). J. Stratigr. 27 (3), 212–215. https://doi.org/10.1016/S0955-2219(02)00073-0 (in Chinese).
Miall, A.D., 1996. The Geology of Fluvial Deposits. Springer Verlag, New York, pp. 251–342. https://doi.org/10.1007/978-3-662-03237-4.
Meng, Q.A., Zhang, S., Sun, G.X., et al., 2016. A seismic geomorphology study of the fluvial and lacustrine-delta facies of the Cretaceous Quantou-Nenjiang Formations in the Songliao Basin, China. Mar. Petrol. Geol. 78, 836–847. https://doi.org/10.1016/j.marpetgeo.2016.01.017.
Nesbitt, H.W., Young, G.M., 1982. Early Proterozoic climates and plate motions inferred from major element chemistry of lutites. Nature 299 (5885), 715–717. https://doi.org/10.1038/299715a0.
Ning, L.X., Zhou, Y.K., Yang, J., et al., 2018. Spatial-temporal variability of the fluctuation of water level in Poyang Lake basin, China. Open Geosci. 10 (1), 940–953. https://doi.org/10.1515/geo-2018-0075.
Olariu, C., Bhattacharya, J.P., 2006. Terminal distributary channels and delta front architecture of river-dominated delta systems. J. Sediment. Res. 76, 212–233. https://doi.org/10.2110/jsr.2006.026.
Overeem, I., Kroonenberg, S.B., Veldkamp, A., et al., 2003. Small-scale stratigraphy in a large ramp delta: recent and Holocene sedimentation in the Volga delta, Caspian Sea. Sediment. Geol. 159, 133–157. https://doi.org/10.1016/S0037-0738(02)00256-7.
Pan, S.X., Wei, P.S., Wang, T.Q., et al., 2012. Sedimentary characteristics of flood-overlake in large depression basin-taking the 4th member, Quantou Formation, lower cretaceous, in southern Songliao Basin as an example. Geol. Rev. 58, 41–52. https://doi.org/10.16509/j.georeview.2012.01.001 (in Chinese).
Postma, G., 1990. An analysis of the variation in delta architecture. Terra. Nova 2, 124–130. https://doi.org/10.1111/j.1365-3121.1990.tb00052.x.
Postma, G., 2001. Physical climate signatures in shallow- and deep-water deltas. Global Planet. Change 28, 93–106. https://doi.org/10.1016/S0921-8181(00)00067-9.
Rahman, A.H.A., Menier, D., Mansor, M.Y., 2014. Sequence stratigraphic modelling and reservoir architecture of the shallow marine successions of Baram field, West Baram Delta, offshore Sarawak, East Malaysia. Mar. Petrol. Geol. 58, 687–703. https://doi.org/10.1016/j.marpetgeo.2014.03.010.
Reading, H.G., 1996. Sedimentary environments: process, facies and stratigraphy. Blackwell Science, Cambridge, pp. 423–429. https://doi.org/10.1038/278486a0.
Sahraeyan, M., Bahrami, M., Arzaghib, Solmaz, 2014. Facies analysis and depositional environments of the Oligocenee miocene asmari formation, Zagros basin, Iran. Geoscience Frontiers. 2014 5 (1), 103–112. https://doi.org/10.1016/j.gsf.2013.03.005.
Sorokin, A.P., Malyshev, Y.F., Kaplun, V.B., et al., 2013. Evolution and deep structure of the Zeya–Bureya and Songliao sedimentary basins (East Asia). Russian Journal of Pacific Geology 7, 77–91. https://doi.org/10.1134/S1819714013020085.
Sun, C.Y., Hu, M.Y., Hu, Z.G., et al., 2017. Characteristics of reservoir sand bodies within high-resolution sequence framework: a case from the 3rd and 4th members of Quantou Formation in Zhou 311 area, northern Songliao Basin. Oil Gas Geol. 38, 1019–1031. https://doi.org/10.11743/ogg20170602 (in Chinese).
Tian, L.X., Liu, H., Niu, C.M., et al., 2019. Development characteristics and controlling factor analysis of the Neogene Minghuazhen Formation shallow water delta in Huanghekou area, Bohai offshore basin. Journal of Palaeogeography. 2019 8 (1), 251–269. https://doi.org/10.1186/s42501-019-0032-8.
Tian, J.C., Chen, G.W., Zhang, X., et al., 2006. Application of sedimentary geochemistry in the analysis of sequence stratigraphy. J. Chengdu Univ. Technol. (Sci. Technol. Ed.) 33 (1), 30–35. https://doi.org/10.3969/j.issn.1671-9727.2006.01.006 (in Chinese).
Wang, C.S., Feng, Z.Q., Zhang, L.M., et al., 2013. Cretaceous paleogeography and paleoclimate and the setting of SKI borehole sites in Songliao Basin, northeast China. Palaeogeogr. Palaeoclimatol. Palaeoecol. 385, 17–30. https://doi.org/10.1016/j.palaeo.2012.01.030.
Wang, J., Cao, Y.C., Liu, H.M., et al., 2015. Formation conditions and sedimentary model of over-flooding lake deltas within continental lake basins: an example from the Paleogene in the Jiyang Subbasin, Bohai Bay Basin. Acta Geol. Sin. 89, 270–284. https://doi.org/10.1111/1755-6724.12410.
Wang, J.H., Chen, H.H., Jiang, T., et al., 2012. Sandbodies frameworks of subaqueous distributary channel in shallow-water delta, Xinli area of Songliao basin. Earth Science 37, 556–564. https://doi.org/10.3799/dqkx.2012.062 (in Chinese).
Wang, J.H., Guan, Z.L., Croix, L.A.D., et al., 2020. Seismic geomorphology of shallow-water lacustrine deltas in the paleocene Huanghua depression, Bohai Bay Basin, eastern China. Mar. Petrol. Geol. 120. https://doi.org/10.1016/j.marpetgeo.2020.104561. Article 104561.
Wang, M.Q., Xie, J., Zhang, Q., et al., 2019. Characteristics and sedimentary model of a reticular shallow-water delta with distributary channels: lower member of the Neogene Minghuazhen Formation in the Bozhong area of the Huanghekou Sag, China. Arabian J. Geosci. 760 (12). http://377.rm.cglhub.com/10.1007/s12517-019-4928-5.
Wei, H.H., Liu, J.L., Meng, Q.R., 2010. Structural and sedimentary evolution of the southern Songliao Basin, northeast China, and implications for hydrocarbon perspectivity. AAPG (Am. Assoc. Pet. Geol.) Bull. 94, 533–566. https://doi.org/10.1306/09080909060.
Wu, H.C., Zhang, S.H., Jiang, G.Q., et al., 2009. The floating astronomical time scale for the terrestrial Late Cretaceous Qingshankou Formation from the Songliao Basin of Northeast China and its stratigraphic and paleoclimate implications. Earth Planet Sci. Lett. 278, 308–323. https://doi.org/10.1016/j.epsl.2008.12.016.
Xi, K.L., Cao, Y.C., Jahren, J., et al., 2015. Diagenesis and reservoir quality of the lower cretaceous Quantou Formation tight sandstone in the southern Songliao Basin, China. Sediment. Geol. 330, 90–107. https://doi.org/10.1016/j.sedgeo.2015.10.007.
Xin, W.Y., Bai, Y.C., Xu, H.J., 2019. Experimental study on evolution of lacustrine shallow-waterdelta. Catena 182, 104125. https://doi.org/10.1016/j.catena.2019.104125.
Yang, L., 2018. Well-logging Inversion on the Palaeoclimate Changes of the Late Cretaceous in Songliao Basin. China University of Geosciences (Beijing), Beijing, pp. 58–71.
You, H.L., Xu, L.G., Liu, G.L., et al., 2015. Effects of inter-annual water level fluctuations on vegetation evolution in typical Wetlands of Poyang lake, China. Wetlands 35, 931–943. https://doi.org/10.1007/s13157-015-0684-9.
Zelilidis, A., Piper, D.J.W., Kontopoulos, N., 2002. Sedimentation and basin evolution of the Oligocene-Miocene Mesohellenic basin, Greece. AAPG (Am. Assoc. Pet. Geol.) Bull. 86, 161–182. https://doi.org/10.1306/61EEDA6C-173E-11D7-8645000102C1865D.
Zeng, C., Yin, T.J., Song, Y.K., 2017. Experimental on numerical Simulation of the impact of lake level plane fluctuation on shallow water delta. Earth Sci. 42 (11), 2095–2104. https://doi.org/10.3799/dqkx.2017.134 (in Chinese).
Zeng, H.L., Zhao, X.Z., Zhu, X.M., et al., 2015. Seismic sedimentology characteristics of sub-clinoformal shallow-water meandering river delta: a case from the Suning area of Raoyang sag in Jizhong depression, Bohai Bay Basin, NE China. Petrol. Explor. Dev. 42, 621–632. https://doi.org/10.1016/S1876-3804(15)30057-4.
Zhao, J., Wan, X.Q., Xi, D.P., et al., 2014. Late Cretaceous palynology and paleoclimate change: evidence from the SK1 (South) core, Songliao Basin, NE China. Sci. China Earth Sci. 57, 2985–2997. https://doi.org/10.1007/s11430-014-4975-4.
Zhao, J.F., Mountney, N.P., Liu, C.Y., et al., 2015. Outcrop architecture of a fluvio-lacustrine succession: upper triassic Yanchang formation, Ordos basin, China. Mar. Petrol. Geol. 68, 394–413. https://doi.org/10.1016/j.marpetgeo.2015.09.001.
Zhang, L., Bao, Z.D., Dou, L.X., et al., 2018. Sedimentary characteristics and pattern of distributary channels in shallow water deltaic red bed succession: a case from the Late Cretaceous Yaojia formation, southern Songliao Basin, NE China. J. Petrol. Sci. Eng. 171, 1171–1190. https://doi.org/10.1016/j.petrol.2018.08.006.
Zhang, L., Bao, Z.D., Lin, Y.B., et al., 2017. Genetic types and sedimentary model of sandbodies in a shallow-water delta: a case study of the first Member of Cretaceous Yaojia Formation in Qian'an area, south of Songliao Basin, NE China. Petrol. Explor. Dev. 44, 770–779. https://doi.org/10.1016/S1876-3804(17)30087-3.
Zhang, X., Lin, C.M., Yin, Y., et al., 2016. Sedimentary characteristics and processes of the paleogene Dainan formation in the gaoyou depression, north Jiangsu basin, eastern China. Petroleum Science. 2016 13 (3), 385–401. https://doi.org/10.1007/s12182-016-0115-4.
Zhao, W., Qiu, L.W., Jiang, Z.X., et al., 2011a. Depositional evolution and model of shallow-water delta in the rifting lacustrine basins during the shrinking stage: a

case study of the third member and second member of paleogene Shahejie formation in the Niuzhuang Subsag, Dongying sag. Acta Geol. Sin. 85, 1019–1027. https://doi.org/10.1007/s12182-011-0118-0 (in Chinese).

Zhao, W.Z., Zou, C.N., Chi, Y.L., et al., 2011b. Sequence stratigraphy, seismic sedimentology, and litho-stratigraphic plays, upper cretaceous, Sifangtuozi area, Southwest Songliao Basin, China. AAPG (Am. Assoc. Pet. Geol.) Bull. 95, 241–265. https://doi.org/10.1306/06301009125.

Zhang, N.N., Wang, W., Wang, Y., 2012. Estimate the area of the Poyang Lake using satellite remote sensing data and analyze its relationship with water level. Remote Sensing Technology and Application 27, 947–953. https://doi.org/10.11873/j.issn.1004-0323.2012.6.947 (in Chinese).

Zhang, S.Y., Liu, Y.X., Yang, Y.H., et al., 2016. Erosion and deposition within Poyang Lake: evidence from a decade of satellite data. J. Great Lake. Res. 42, 364–374. https://doi.org/10.1016/j.jglr.2015.12.012.

Zhu, W.L., Li, J.P., Zhou, X.H., 2008. Neogene shallow water deltaic system and large hydrocarbon accumulations in Bohai Bay, China. Acta Sedimentol. Sin. 26, 575–582. https://doi.org/10.14027/j.cnki.cjxb.2008.04.016 (in Chinese).

Zhu, X.M., Liu, Y., Fang, Q., et al., 2012. Formation and sedimentary model of shallow delta in large-scale lake, example from cretaceous Quantou Formation in Sanzhao sag, Songliao Basin. Earth Sci. Front. 19, 89–99. CNKI:SUN:DXQY.0.2012-01-012 (in Chinese).

Zhu, X.M., Deng, X.Q., Liu, Z.L., et al., 2013a. Sedimentary characteristics and model of shallow braided delta in large-scale lacustrine: an example from Triassic Yanchang Formation in Ordos Basin. Earth Sci. Front. 20, 19–28. CNKI:SUN:DXQY.0.2013-02-005 (in Chinese).

Zhu, X.M., Pan, R., Zhao, D.N., et al., 2013b. Formation and development of shallow-water deltas in lacustrine basin and typical case analyses. Journal of China University of Petroleum 37, 7–14. https://doi.org/10.3969/j.issn.1673-5005.2013.05.002 (in Chinese).

Zhu, X.M., Li, S.L., Wu, D., et al., 2017a. Sedimentary characteristics of shallow-water braided delta of the Jurassic, Junggar basin, Western China. J. Petrol. Sci. Eng. 149, 591–602. https://doi.org/10.1016/j.petrol.2016.10.054.

Zhu, X.M., Zeng, H.L., Li, S.L., et al., 2017b. Sedimentary characteristics and seismic geomorphologic responses of a shallow-water delta in the Qingshankou Formation from the Songliao Basin, China. Mar. Petrol. Geol. 79, 131–148. https://doi.org/10.1016/j.marpetgeo.2016.09.018.

Zou, C.N., Tao, S.Z., Gu, Z.D., 2006. Formation conditions and distribution rules of large lithologic oil–gas fields with low abundance in China. Acta Geol. Sin. 80, 1739–1751. https://doi.org/10.1111/j.1745-4557.2006.00081.x (in Chinese).

Zou, C.N., Zhao, W.Z., Zhang, X.Y., et al., 2008. Formation and distribution of shallow-water deltas and central-basin sandbodies in large open depression lake basins. Acta Geol. Sin. 82, 813–825. https://doi.org/10.3321/j.issn:0001-5717.2008.06.011 (in Chinese).